出國報告（出國類別：國際研討會）

出席「第四屆先進材料及奈米技術國際會議（ICAMN IV 2016）」心得報告

服務機關：國防大學理工學院化學及材料工程學系
姓名職稱：文職教授　汪成斌
派赴國家：馬來西亞
出國期間：105 年 11 月 9 日至 11 月 11 日
報告日期：105 年 11 月 28 日

摘要

第四屆先進材料及奈米技術國際會議（ICAMN IV 2016）是由馬來西亞大學科學院奈米材料研究中心主辦，於 2016 年 11 月 9 - 11 在蘭卡威灣景酒店舉行，為先進材料之開發領域重要的國際會議之一。會議共舉行三天，每天行程滿檔（09:00 至 17:00），計有大會專題演講（共 8 位），各相關主題(電化學材料、電氣電子材料、生物，醫學和藥物、材料與技術、半導體和超導材料、催化材料、光敏材料、奈米材料和奈米結構、聚合物材料和複合材料、金屬和合金、核材料和輻射材料、理論和模擬等)之邀請講座（共 13 位），另提供口頭和壁報論文之發表。吸引了超過 100 名來自世界各地的學者，包括希臘、德國、瑞士、土耳其、英國、印尼、印度、摩爾多瓦、沙烏地阿拉伯、新加坡、馬來西亞、香港、泰國、韓國、日本、中國、台灣等，此研討會投稿論文分口頭報告（共 70 篇）及壁報展示（共 30 篇），共計 100 篇，為一中小型國際會議。在會議中聆聽各國學者之學術演講，並於茶敘交流時間彼此交換意見並討論相關問題。本次會議提供一個相當好的知識交流及科學合作的聯網平台，各國學者齊聚一堂研討各種先進材料領域最新之進展和技術信息，並傳達新的研究領域和國際未來發展方向及其優先次序。此外藉由參與大會各國專家學者之交換研究心得及吸取他人寶貴之研究經驗，亦可做為本實驗室日後研究之參考。

筆者感謝科技部之經費補助本人及二位碩班研究生成行，計發表一篇口頭報告論文：“Catalytic Performance of Carbon Monoxide Oxidation over Nanostructured Cobalt Oxides”，及二篇壁報展示論文：“Evaluation of CO Oxidation over Co_3O_4-supported NiO Catalysts”、“Graphene Sponge as an Efficient and Recyclable Oil Sorbent”，達到與各國學者切磋交流的機會，真是獲益匪淺。

目次

頁碼

壹、 會議目的

第四屆先進材料及奈米技術國際會議（ICAMN IV 2016）是由馬來西亞大學科學院奈米材料研究中心主辦，於 2016 年 11 月 9 - 11 在蘭卡威灣景酒店舉行，為一跨學科國際會議。本次會議提供一個相當好的知識交流平台，各國學者齊聚一堂研討各種先進材料領域近期之成果、新穎應用於奈米材料之鑑定設備及未來之進展和技術信息，並傳達新的研究領域和國際未來發展方向及其優先次序。會議宗旨在於藉由學術的發展與腦力激盪，借鑒實證研究和概念的見解，達到共享交流。依專長領域進行一系列學術研究成果發表及新知討論，以便交流最新進展和技術信息，歷年來相關之學術研討會及專題討論會，皆對該學術領域有深遠的影響及貢獻。因此，藉由此學術交流進而瞭解國際未來研究發展方向及趨勢，並與各國專家學者交換研究心得及吸取他人寶貴經驗是很不錯的體驗，將可做為日後研究題材之參考。

貳、 會議過程

本會議屬於一中小型國際研討會，於2016年11月9 - 11日在蘭卡威灣景酒店舉行，參加人員超過100員，分別來自世界各國之學術單位、民間機構、專家學者及研究人員參與為期三天之學術論文發表討論會。大會所討論之範圍很廣，包含電化學材料、電氣電子材料、生物，醫學和藥物、材料與技術、半導體和超導材料、催化材料、光敏材料、奈米材料和奈米結構、聚合物材料和複合材料、金屬和合金、核材料和輻射材料、理論和模擬等，與會者多為各國在該領域學有專精之工程師、技術員、教授、研究生與學者，本次台灣參與之人員僅六位教授及研究生（包含台大、成大、同步輻射中心及國防大學等）。於研討會期間與各學者相互密切交流之下獲益良多。蘭卡威為一離島觀光勝地，需搭機至吉隆坡，再轉搭馬來西亞國內航班至蘭卡威，雖非暑假期間，出團的旅客還是非常多，且轉機班次銜接不順，花了一天時間才抵達會議現場（09:30 – 19:30），並入住灣景酒店。三天與會期間過程十分順利，由於每天議程都有不同主題分別在不同的場地同時進行，因而無法全面顧及，謹將本人出席參與的部分簡要介紹如下。

11月9日（大會第一天）

大會第一天安排了四場相當精采的大會專題演講，及分組（催電化學材料、電氣電子材料、生物，醫學和藥物、材料與技術、半導體和超導材料等）的研討議題。第一場大會專題演講邀請石原達己（Tatsumi Ishihara）教授（九州大學應化系兼國際研究所副所長）主講「Solid Oxide Reversible Cells Using $LaGaO_3$-Based Oxide Electrolyte and Oxide Fuel Electrode」，印象最深刻。石原達己教授為國際SOFC知名學者，其研究團隊在LSGM-based之低溫型固態氧化物燃料電池的技術開發在國際間極富盛名。日本學術振興會（Japan Society for the Promotion of Science）的世界頂尖研究中心計畫（World Premier International Research Center Initiative, WPI）於2007年由文部科學省開始成立，鼓勵日本的大學與世界一流大學/機構合作在日本境內成立頂尖研究中心，提供大量經費，建構頂尖儀器設施與優良研究環境，吸納全球人才，其目的為促進日本之科技發展。九州大學於2010年加入此項WPI頂尖研究中心計畫，與美國伊利諾大學香檳分校合作成立I^2CNER（International Institute for Carbon-Neutral Energy Research）研究中心，目前石原教授為此中心之副執行長。I^2CNER研究中心鼓勵國際合作，石原教授帶領的是一個非常龐大的研究團隊，總體研究人力資源超過50人。除了多套燃料電池製程設備與電性效能測試儀器之外，並主持九州大學所擁有之一個燃料電池實地驗證測試場，可提供多家業者的ENE-FARM系統進行測試驗證計畫，另其實驗室擁有多項精密材料分析設施，如SIMS、XPS、STEM、ESR、XRD、q-Tac、FIB-SEM 等貴重分析設施，學術成就優良，因此石原教授與許多國際學者有密切的合作交流。同時，亦與相關業界緊密結合，TOTO與Kyocera等SOFC業者與石原教授也有相關合作計畫並進行頻繁的技術合作。日本在SOFC技術的發展上，有著周延的燃料電池發展規劃，涵蓋大、中、小型SOFC發電系統開發，相關的技術開發應用由新能源及產業技術發展組織NEDO（1980年成立）主導，2004 ~ 2007發展目標為驗證系統耐用性及可靠度評估；小型kW級SOFC家用熱電共生系統（Combined Heat & Power, CHP）在2007年以後進行小規模測試。另NEDO投入燃料電池&氫能研發工作30年，2014年首將氫能燃料電池定為日本重要之Future Secondary Energy，2014年中日本經濟產業省亦制定「氫能、燃料電池戰略藍圖，第一階段自即日起至2025年，主要為安裝微熱電燃料電池系統、燃料電

池車及大型熱電燃料電池系統；第二階段於2020 ~ 2030年建構氫氣供電系統及氫氣量產產業13鏈；第三階段自2040年起，建構無二氧化碳排放之氫能供應系統。NEDO同時並進行SOFC之商品化推展（2013 ~ 2017），其小型SOFC發電系統主力為700 W，適於日本居家使用。另日本燃料電池車已發表，惟目前加氫站數量不多，以福岡市為例僅有三座（一座位於九州大學內），日本東京將於2020年舉辦奧運會，屆時東京預估將建造完成200座加氫站提供燃料電池車輛使用。在分項演講中印象最深刻的是Yoshimitsu Uemura學者的論文「Nano-catalysts for Upgrading Bio-oil: Catalytic Decarboxylation and Hydrodeoxygenation」發表。近來原油價格的變化及燃燒化石原料對環境之嚴重衝擊，發展再生能源已是全球努力的方向及重要方針，目前生質柴油的生產方式皆採用轉酯化製程，為提高轉化率，反應時間長達一小時。反應時採用強鹼作催化劑，反應後需設立廢水處理系統，工廠操作成本高。本篇報告採用加氫飽和及加氫脫氧的方式，飽和棕櫚油中的烯烴和脫除其中的氧原子，實驗應用固有的加氫脫硫設備，添加棕櫚油至一般柴油進料中，經由加氫脫硫設備，將棕櫚油中的烯烴飽和及氧原子脫除，形成正烷烴的碳氫化合物。這些正烷烴的碳氫化合物和柴油中的成份相同，而且正烷烴的碳氫化合物含有高的十六烷值指數，可提高原有柴油進料中的十六烷值指數。在加50wt%的棕櫚油至柴油進料中時，柴油產品的十六烷值指數可由不含棕櫚油的57提高到70。藉由貴重儀器對系列材料之結構做一詳盡探討，評估其應用效能，獲得在座學者熱烈的迴響並提出不同觀點，Yoshimitsu Uemura學者均能詳加解說。我們實驗室正準備踏入此項研究，目前僅設計並合成出系列酸、鹼觸媒（La_2O_3、CaO、CaO-La_2O_3），初步成果顯示具有催化效果。趁中場休息時間請教Yoshimitsu Uemura學者，建議我們可以改變金屬先驅物、調控酸鹼值，回國後將依建議嚐試。另壁報展示安排在今天和明天，利用會議期間安排之茶敘時間進行交流，期間有多位學者對我們的研究內容有興趣而提出不同觀點，相互討論、切磋，真是獲益匪淺。綜整各學者提供之建議如下：複合氧化物之鑑定及其活性關聯性需再確認、一氧化碳氧化之機制需做修正、金屬含量需精確量測、石墨烯海綿的吸收有機溶劑和油脂機理需詳述、墨烯海綿再生應用需加強其效率。感謝各學者之建議，擬於近期內將文章撰寫完成並投稿至“Journal of Energy and Power Engineering”及“Nanotechnology”。

11月10日（大會第二天）

大會第二天安排了二場相當精采的大會專題演講，及分組（催化材料、光敏材料、奈米材料和奈米結構等）的研討議題。其中一場大會專題演講邀請台大化工系吳乃立教授主講「Progress Toward High Energy Nanocrystalline Oxide Supercapacitors」，印象最深刻。吳教授研究工作主要集中在三大重點領域，包括電化學能量存儲材料與元件的開發，包括超級電容器和鋰離子電池（開發兼具有高電容量之奈米晶型與奈米結構之電極材料）；基於同步加速器設施，發展應用於能源材料和元件的先進原位分析方法；奈米晶型金屬氧化物之合成與分析（開發量產全結晶奈米小於10 nm晶型與中孔結構之金屬與氧化物粉體與膠體之製程，並探討此類物質所顯現出之特異相穩定與電子、電化學性質）。另最新的研究包含高功能電化學元件材料之先進製程、綠色化學程序尖端技術-超重力化工程序應用之研發、用靜電紡絲合成鋰離子電池高容量負極纖維、儲能電極開發與應用等，在新興科技領域的傑出貢獻而榮獲第十四屆「有庠科技論文獎（綠色科技類）」，其豐碩學術研究成果獲得高度肯定。吳教授報告內容包含(1)奈米晶粒鋰離子正極氧化物的製備：鋰離子正極氧化物可應用至水電解質之混成超高電容系統，能有效提高（~50%）能量密度。鋰離子在水溶液中溶解度大（高達5 N以上），其離子導電度很高，適用於極高功率的超高電容器應用。另開發水溶液化學製程，搭配高導電碳材(管)，製備兼具高速充放電能力與長循環壽命之新型鋰離子正極氧化物複合材料。(2)開發新型有機電解質法拉第超高電容材料：具法拉第「偽電容」之超高電容材料，具有較電雙層電容更高的比電容量。已知的偽電容材料僅限於水系電解質系統，唯一應用於有機電解質的材料係為吳教授開發之錳鐵氧化物。若使用有機電解質可將電容器之電壓操作範圍由1.2 V提升至約3.0 V，電容密度將增加數倍。偽電容材料結構以無晶型或奈米晶型為主，並以鋰離子嵌入/出作動之偽電容材料。由於超級電容材料之開發是目前很熱門的研究主題，在座的學者提出了許多不同的論點與質疑，吳教授均能詳細的解釋，具有大師風範。在分項演講中印象最深刻的是馬來西亞Taufiq Yap教授的論文「Nanocatalysts for Sustainable Bioenergy Production」發表，由於石油的儲量日逐漸減少及國際原油價格的波動有，各國紛紛尋找可替代能源及替代燃料。目前，已經能上場替代石油使用的便是「生質柴油」，生質柴油為再生能源的一種，亦屬

於清潔能源，具有生物可分解性及再生循環的特色。雖然目前業界已能利用均相轉酯化反應，大量地生產生質柴油，然該程序仍存在有某些缺點，如純化過程需經中和、蒸餾及水洗等程序。在此程序中，將產生大量廢水，而易對環境造成二次負擔之缺點。因此Taufiq Yap教授團隊利用非均相觸媒進行轉酯化反應，發展方便使用且不易造成環境污染的固體觸媒。 芥花油為目前廣範使用於潤滑油之原料，相對於其它含脂肪酸之原料油（如大豆油、葵花油）而言，其具有價格便宜、容易取得等優點；然在過去文獻中，鮮少有學者選用芥花油做為生質柴化轉酯化反應之原料，故其團隊選用芥花油為原料，探討適合其進行生質柴油轉酯化的反應條件。反應條件包含：活性相種類（NaOH、$Ca(OH)_2$）、擔體種類（Al_2O_3、水滑石）、含浸液種類、含浸時間、活性相附載量等觸媒製備參數對生質柴油轉化率的影響。我們實驗室正準備踏入此項研究，相關內容是很重要的考資料，因Taufiq Yap教授報告完即離開，錯過交談的機會，回國後將閱讀Taufiq Yap教授發表的系列文章，再構思研究方向。下午是實驗室呈現成果的重頭戲，由我口頭報告論文「Catalytic Performance of Carbon Monoxide Oxidation over Nanostructured Cobalt Oxides」，吸引了許多學者提問並建議盡速撰寫文章投稿，回國後已收到「Journal of Energy and Power Engineering」期刊邀稿。感謝各學者所提建言，回饋了我們許多思考空間，擬於近期內待新年度科技部之研究計畫申請案完成後，著手整理撰寫文章。

<u>11月11日</u>（大會第三天）

大會第三天安排了二場大會專題演講，及分組（聚合物材料和複合材料、金屬和合金、核材料和輻射材料、理論和模擬等）的研討議題。其中一場大會專題演講邀請台灣同步輻射中心湯茂竹博士主講「X-ray Nanoprobe at Taiwan Photon Source: Probing Towards the World of Nanometers」，同步輻射在基礎科學、應用科學和工藝學等領域已得到廣泛應用，如測定蛋白質的結構和蛋白質的分子結構,通過X射線小角散射可研究蛋白質生理活動過程和神經作用過程等的動態變化；可用於研究固體的表面性質，如半導體和金屬表面的光特性，物質的氧化、催化、腐蝕等過程的表面電子結構和變化；可用於測定原子的配位結構、大分子之間的化學鍵參數等。湯博士逐一介紹在台灣光子源中的次微米繞射及奈米探測光束線的新穎技術，包含三維奈米勞厄繞射、X光吸收、X光螢光、X光光激螢光光譜、穿透X光顯微術及X光結合掃

描探針顯微術等；並介紹台灣光子源在奈米探測實驗站之設計及未來應用、次微米繞射實驗站的設計，該平台將可為中心用戶帶來同域整合分析的可能性，在技術、設施及應用上可作為將來台灣光子源兩座奈米分析相關實驗站的發展依據。蘭卡威灣景酒店會議中心有好幾個中、小型會議廳，共可容納將近400人，這次大會使用了一個中型會議廳及二個小型會議廳。整個會議中心還包含住宿、餐廳，且臨海是不錯的開會、度假勝地，唯會議期間天氣炎熱、每天都有午後局部雨，是令人美中不足之處。第三天中午會議結束即刻換裝步行至蘭卡威著名地標：瓜鎮老鷹廣場（Eagle Square）一遊，蘭卡威的Lang是馬來文的「老鷹」（helang），kawi則是「赤紅色」的意思，靠近碼頭旁的廣場上所佇立的紅赤色大老鷹即代表了蘭卡威。這隻赤紅色大老鷹耗費110萬馬幣（約合35萬美金）打造，從頭至腳部約12.6公尺，雙翅展開答21.6公尺，是以鋼固水泥作為主體，外包玻璃纖維。老鷹身上的紅棕色羽毛則是一片片黏上去的銅片，做工精細，頭部為白色，鼻翼處呈水藍色，目光炯炯有神。這座老鷹廣場是由設計市政廳的李金友建築師打造的，從天空鳥瞰廣場，形狀有如兩個連結的三角形，靈感出自馬來西亞的風箏造型。

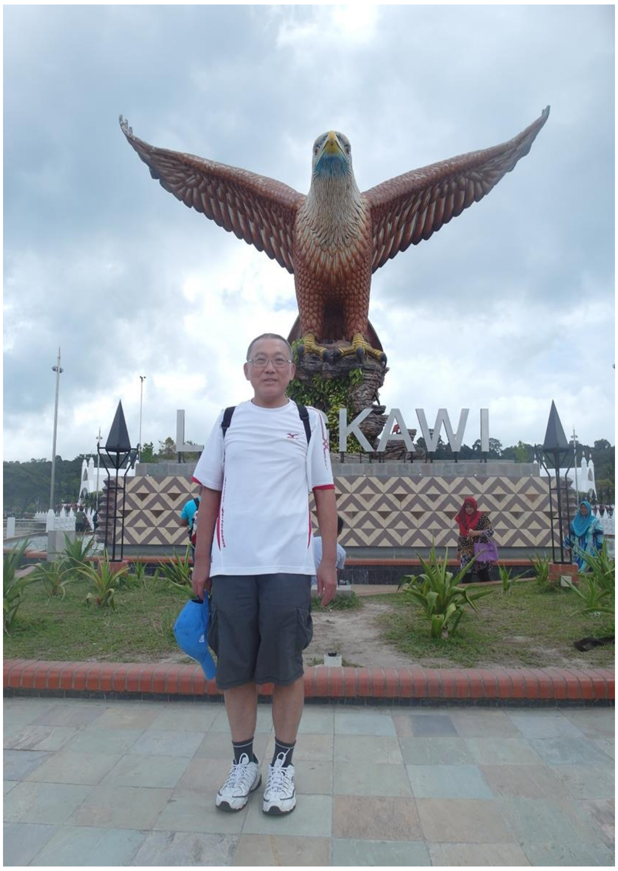

參、 會議心得

本研討會為一跨學科國際會議，主題涵蓋電化學材料、電氣電子材料、生物，醫學和藥物、材料與技術、半導體和超導材料、催化材料、光敏材料、奈米材料和奈米結構、聚合物材料和複合材料、金屬和合金、核材料和輻射材料、理論和模擬等的工程師、技術員、教授、研究生與學者，就專長領域進行一系列學術研究成果發表及新知討論。會議是由馬來西亞大學科學院奈米材料研究中心主辦的學術會議，參加人員為世界各國之專家學者，此研討會投稿論文分口頭報告及壁報展示，共計100餘篇。大會所討論之範圍很廣，包含能源、綠色工程、環境催化、先進多功能材料等，且相關論述主題亦十分具參考價值。

本人及二位碩班研究生參與會議並有一篇口頭報告及二篇壁報論文發表，透過各國學者不同領域的經驗，於問答間各取所需，達到知識精進功效，並積極與各國學者交換演講意見達到學術交流目的。本次會議提供一個相當好的知識交流平台，藉由此學術交流進而瞭解國際未來研究發展方向及趨勢，真是獲益匪淺。

肆、 建議事項

第四屆先進材料及奈米技術國際會議（ICAMN IV 2016）於 2016 年 11 月 9 - 11 在蘭卡威灣景酒店舉行，為先進材料之開發領域重要的國際會議之一。探討範圍包含能源、綠色工程、環境催化、先進多功能材料等，值得相關研究人員與學者參與。這次研討會馬來西亞參與人數最多，超過 70 員，台灣參加人數僅 6 員。出席國際學術會議情況是大學辦學績效評估中非常重要的指標參考依據，各校應積極鼓勵研究生及老師踴躍出席國際學術會議，以展現研究成果之決策應該持續推動。本人參加這次會議，發現除主辦國，泰國、印度、日本、韓國等國家之出席人數均高出我們許多，鄰近國家重視全方位科學研究與發展之務實態度值得借鏡。個人認為學校鼓勵作法仍可加強，譬如提供更多的經費補助，以鼓勵並增加國內專家學者參與機會，藉以吸收國際新知並分享研究成果，相信對國內各方面研究及學術工作的提昇，必定有所助益。願以此次的與會心得與大家分享，本次研討會攜回會議論文冊乙本。

作者發表之論文

Catalytic Performance of Carbon Monoxide Oxidation over Nanostructured Cobalt Oxides

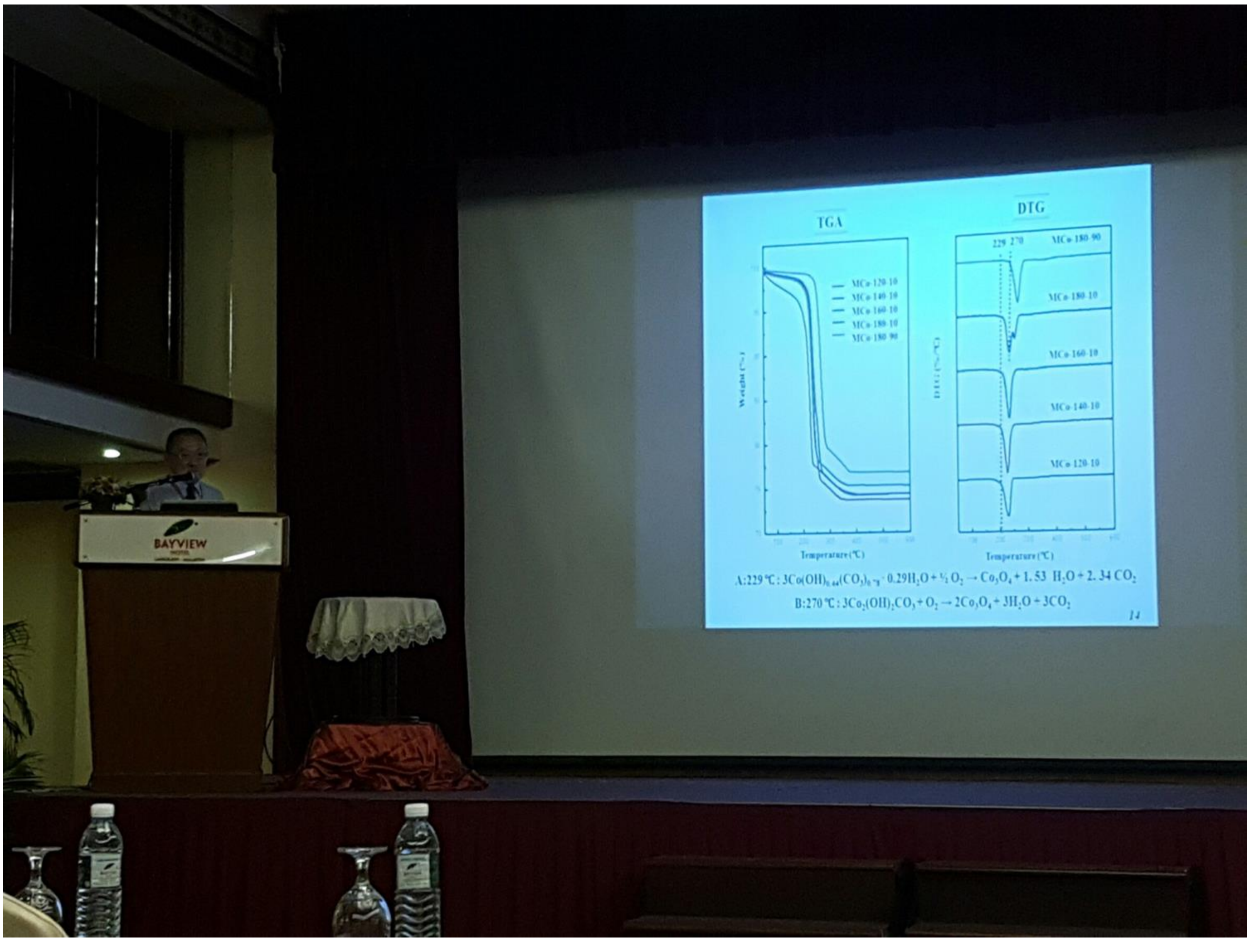

Catalytic Performance of Carbon Monoxide Oxidation over Nanostructured Cobalt Oxides

Chen-Bin Wang
National Defense University, Taiwan

11/10/2016 in Langkawi, Malaysia (ICAMN IV 2016)

Sources of CO Pollutants

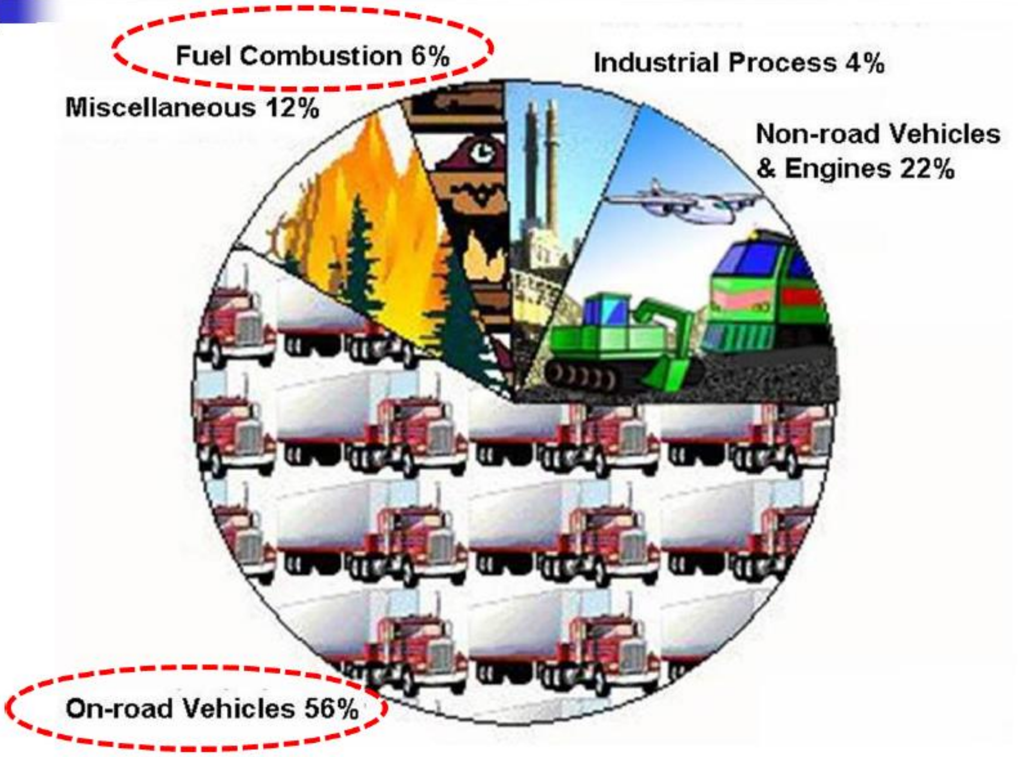

www.epa.gov/air/urbanair/co/what1.html

Survey of Literatures

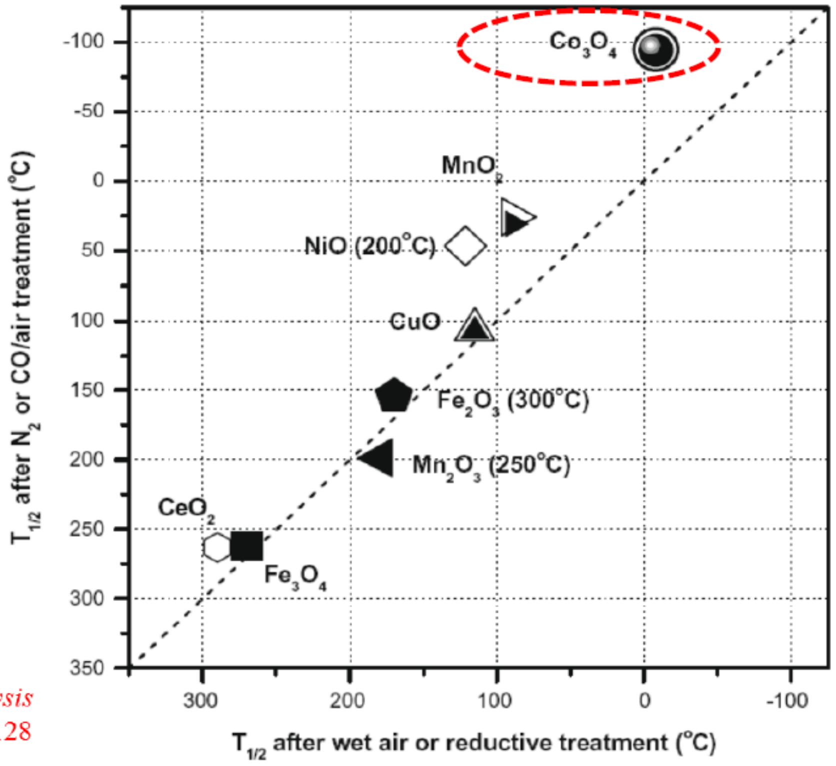

Journal of Catalysis 267 (2009) 121–128

Survey of Literatures

	Catalysts	methods	T_{50} (°C)	S_{BET} ($m^2 \cdot g^{-1}$)	Reference
M/S	5%Pd/CeO$_2$	Microwave	140	—	J. Phys. Chem. B, 109 , 17351 , (2005)
	5%Pd/CuO		131	—	
	5%Pd/ZnO		194	—	
	Pt/γ-Al$_2$O$_3$	Incipient wetness impregnation	233	66	Applied Catalysis B 54 183, (2004)
	Pt/CeO$_2$		56	64	
	Pt/CeO$_2$/γ-Al$_2$O$_3$		94	52	
	1%Pt/Cs-Zeolite Y	Impregnation	82	542	J. Phys. Chem. B 109, 3822, (2005)
	1%Pt/K-Zeolite Y		117	690	
	Au/Fe$_2$O$_3$ –C400	Co-precipitation	< 0 (100%)	37	J. Catal. 144, 175, (1993)
	Au/Co$_3$O$_4$ –C400	Deposition-precipitation		59	
	Au/TiO$_2$ –C400			50	
	3%Au/ Co$_3$O$_4$	Co-precipitation	-22(100%)	—	J. Mol. Catal., 17, 264, (2003)
MO$_x$	CeO$_2$/ZrO$_2$	Sol-gel	340	—	Catal. Today 68, 53, (2001)
	NiO/CeO$_2$	Co-precipitation	241	50	Appl. Catal. A 251, 143, (2003)
	CeO$_2$/SnO$_2$	Co-precipitation	200	—	Catal. Lett., 71, 69, (2001)
	MoO$_3$/CeO$_2$	Impregnation	125	96	Appl. Catal. A287, 236, (2005)
	CoO$_x$/CeO$_2$	Co-precipitation	125	44	Applied Catalysis A 251, 143, (2003)
	CeO$_2$/Co$_3$O$_4$	Impregnation	**88**	**109**	Apply Catalysis **A309, 37-43 (2006).**

Nanostructures of Cobalt Oxides

(Nanoparticles)

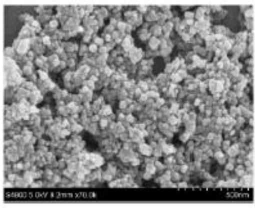

Chem. Commun., (2002) 1486

(Nanorods)

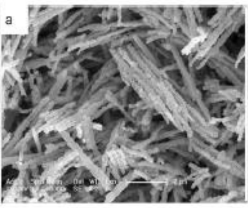

J. Phys. and Chem. Solids 70 (2001) 847

(Nanotubes)

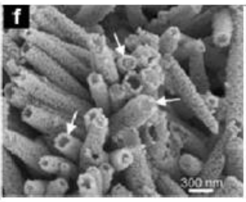

Adv. Mater. , 20 (2008) 258

(Nanowires)

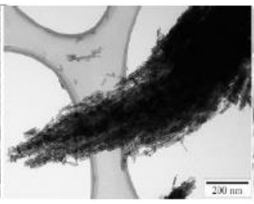

Nano Lett., 6 (2006) 12

(Nanofibers)

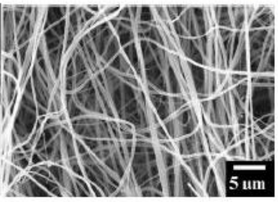

J. Phys. Chem. C, 112 (2008) 12225

(Nanowalls)

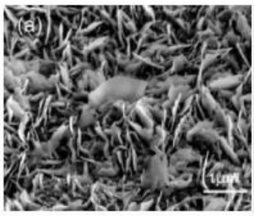

Advanced Materials 17 (2005) 1595

(Nanosheets)

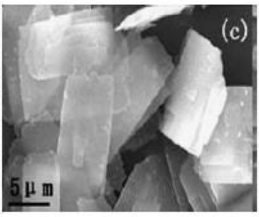

Journal of Alloys and Compounds, 476 (2009) 739

(Nanotube arrays)

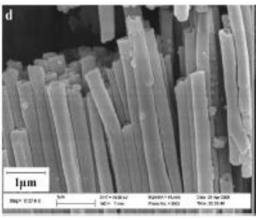

Materials Letters, 63 (2009) 578

(Mircospheres)

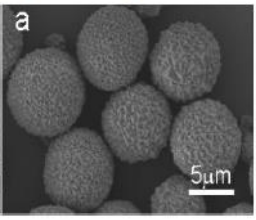

Crystal Growth & Design, 9 (2009) 210

(Flower-Like)

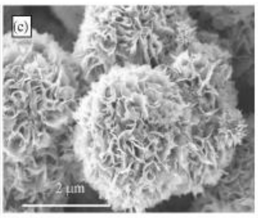

J. Phys. Chem. C, 112 (2008) 8177

Motivation and Goal

Motivation

Abatement of Carbon Monoxide

Goal

Preparation of Nanostrutured Cobalt Oxides

T_{50} for CO oxidation below 0 °C

Catalytic Performance: CO Oxidation

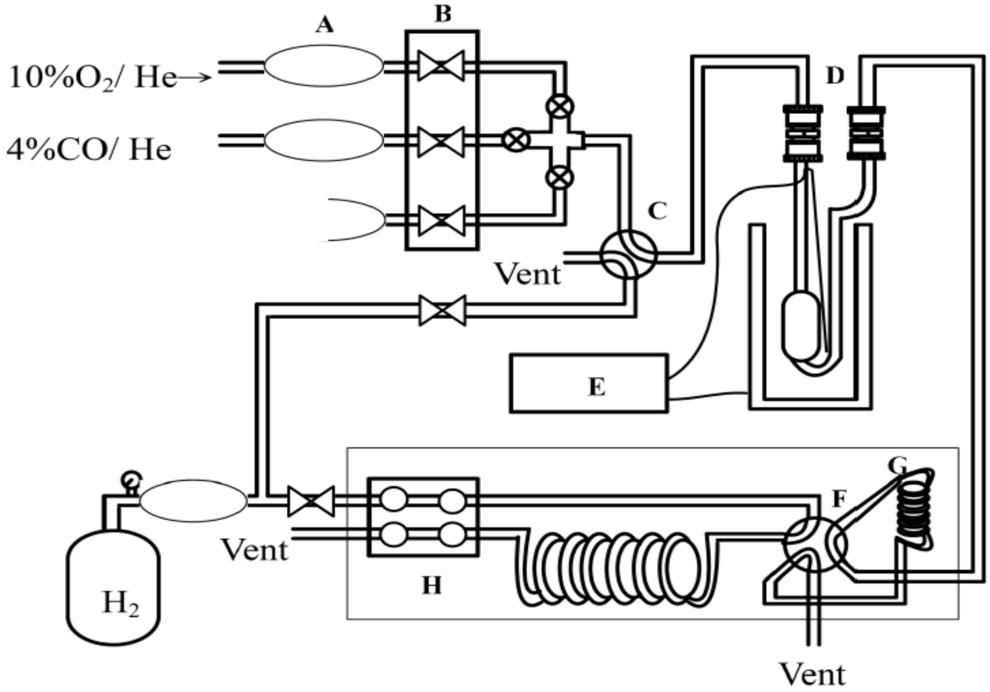

A : Silica Gel
B : Mass Flow Meter/ Controller
C : 4-Way Valve
D : Reactor
E : Temperature Programmed Controller
F : 6-Way Valve
G : Sampling Loop
H : TCD Detector

Preparation of Catalysts : Microwave Hydrothermal

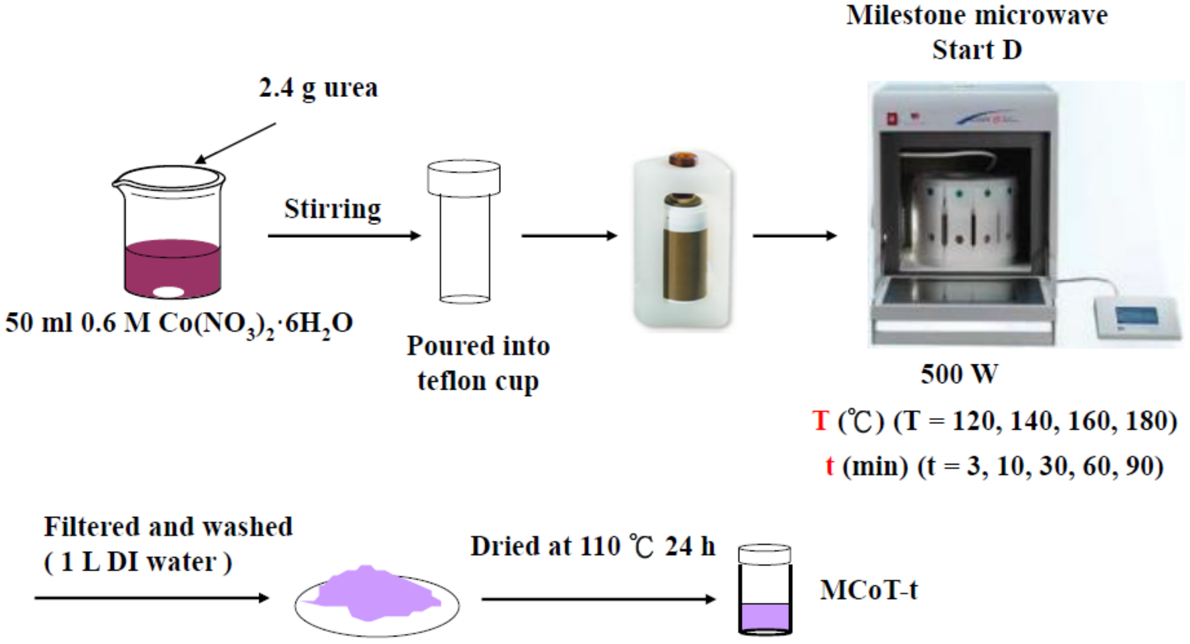

Milestone microwave
Start D

2.4 g urea

Stirring

50 ml 0.6 M $Co(NO_3)_2\cdot 6H_2O$

Poured into
teflon cup

500 W

T (℃) (T = 120, 140, 160, 180)

t (min) (t = 3, 10, 30, 60, 90)

Filtered and washed
(1 L DI water)

Dried at 110 ℃ 24 h

MCoT-t

XRD Characterization

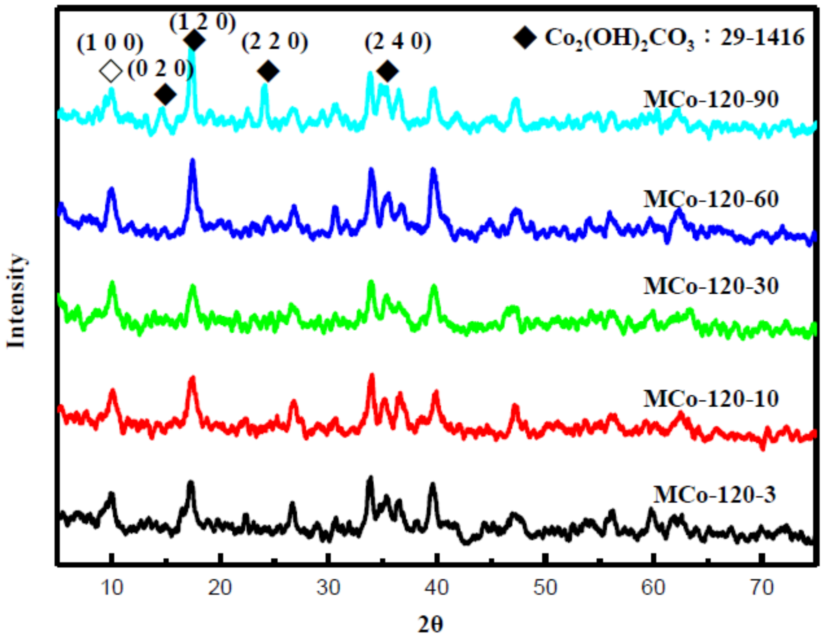

B : Monoclinic cobalt hydroxide carbonate

$Co_2(OH)_2CO_3$

$[Co(OH)_2\cdot CoCO_3]$

A : Hexagonal cobalt hydroxide carbonate

$Co(OH)_{0.44}(CO_3)_{0.78}\cdot 0.29H_2O$

XRD Characterization

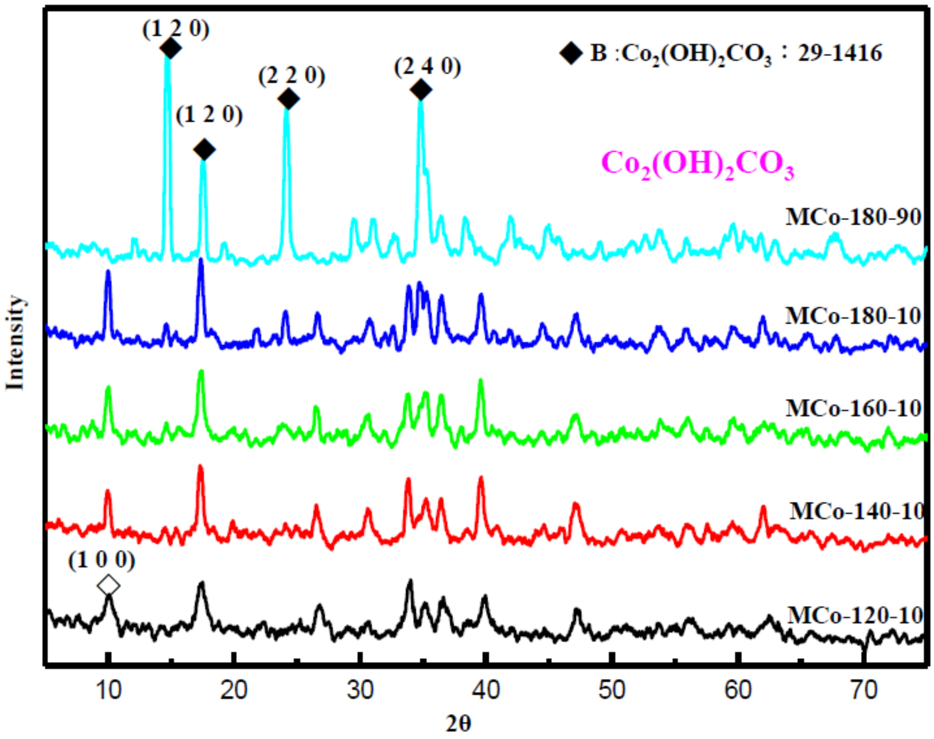

XRD Characterization

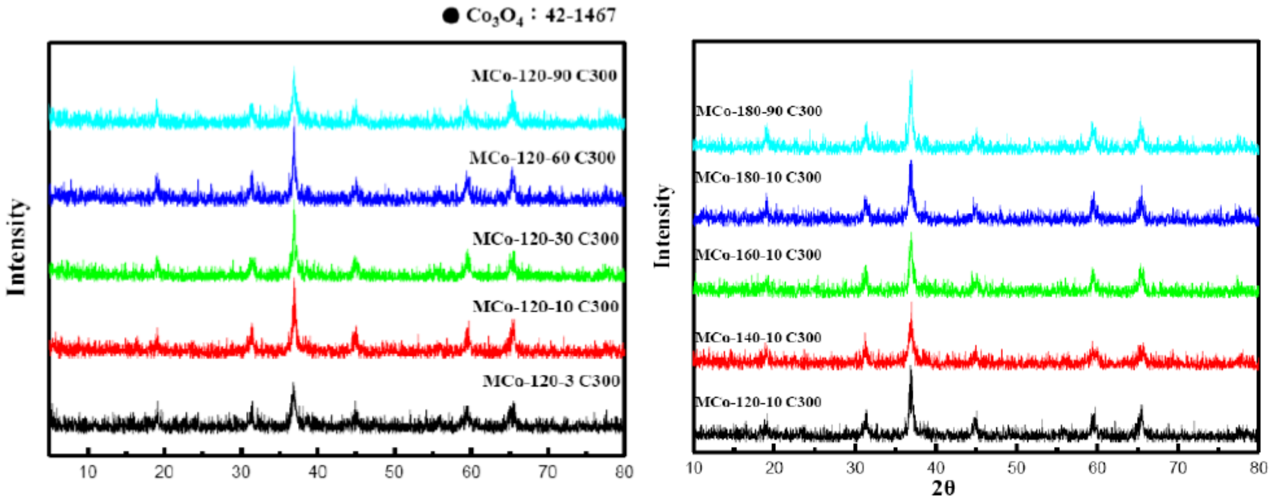

(Calcination temperature : 300 ℃ in air for 1 h)

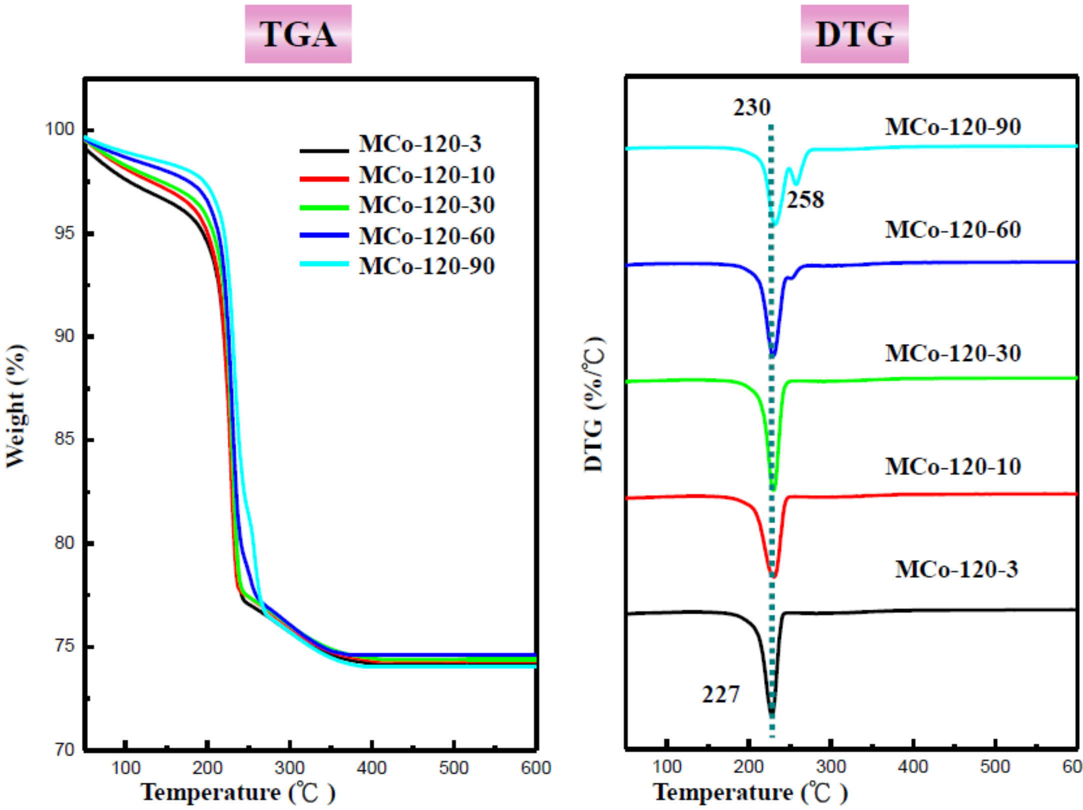
TGA

DTG

A: 230 ℃ : $3Co(OH)_{0.44}(CO_3)_{0.78} \cdot 0.29H_2O + \frac{1}{2} O_2 \rightarrow Co_3O_4 + 1.53\ H_2O + 2.34\ CO_2$

B: 258 ℃ : $3Co_2(OH)_2CO_3 + O_2 \rightarrow 2Co_3O_4 + 3H_2O + 3CO_2$

TGA

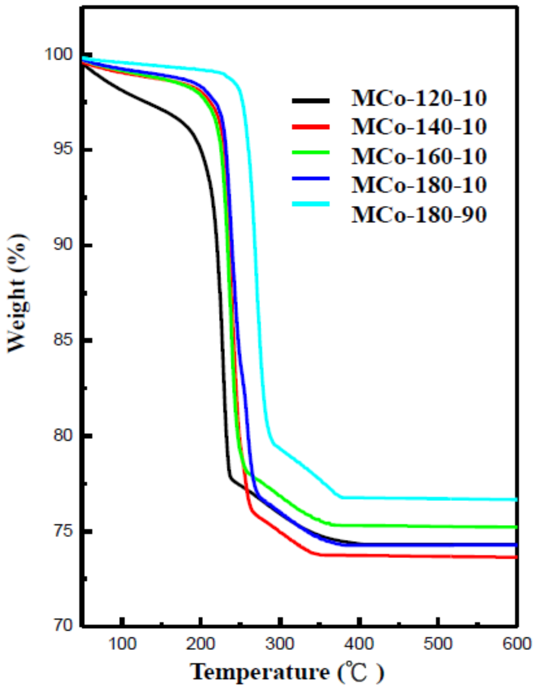

DTG

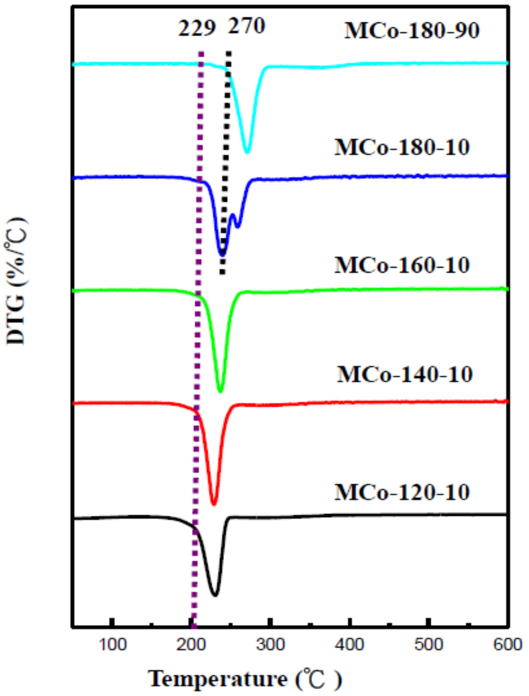

A:229 ℃ : $3Co(OH)_{0.44}(CO_3)_{0.78} \cdot 0.29H_2O + \frac{1}{2} O_2 \rightarrow Co_3O_4 + 1.53\ H_2O + 2.34\ CO_2$

B:270 ℃ : $3Co_2(OH)_2CO_3 + O_2 \rightarrow 2Co_3O_4 + 3H_2O + 3CO_2$

TPR Characterization

B: $Co_2(OH)_2CO_3 + 2H_2 \rightarrow 2Co + 2H_2O + H_2CO_3$

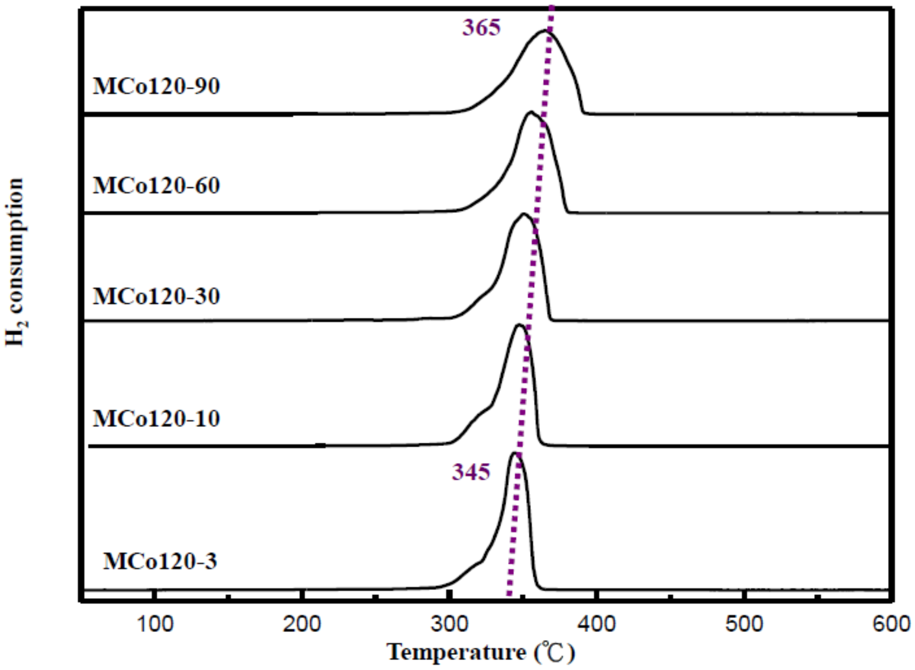

A: $Co(OH)_{0.44}(CO_3)_{0.78} \cdot 0.29H_2O + H_2 \rightarrow Co + 0.73H_2O + 0.78\ H_2CO_3$

TPR Characterization

B: $Co_2(OH)_2CO_3 + 2H_2 \rightarrow 2Co + 2H_2O + H_2CO_3$

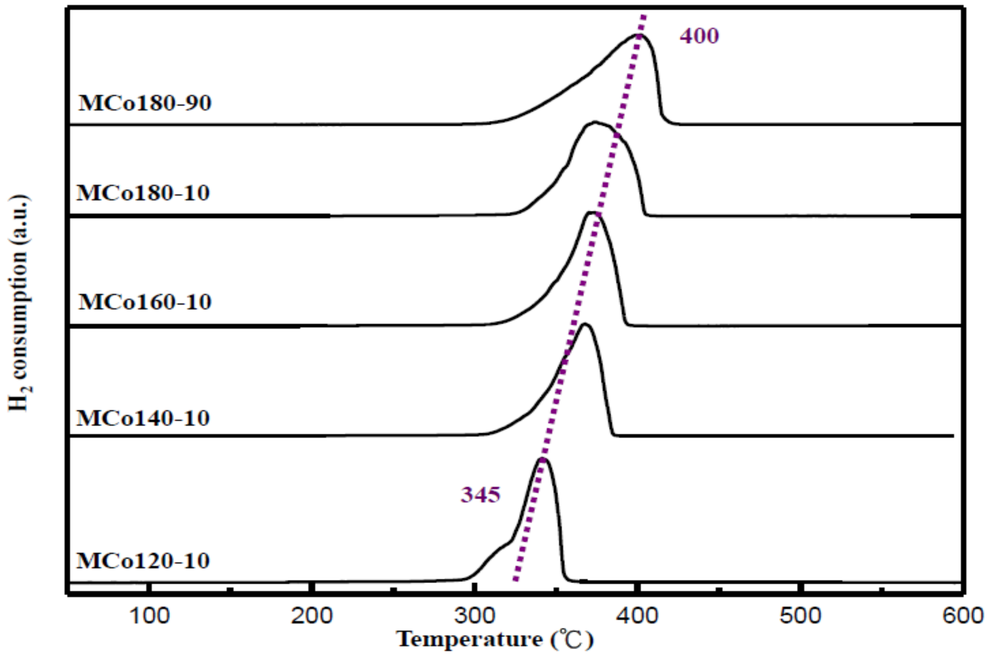

A: $Co(OH)_{0.44}(CO_3)_{0.78} \cdot 0.29H_2O + H_2 \rightarrow Co + 0.73H_2O + 0.78\ H_2CO_3$

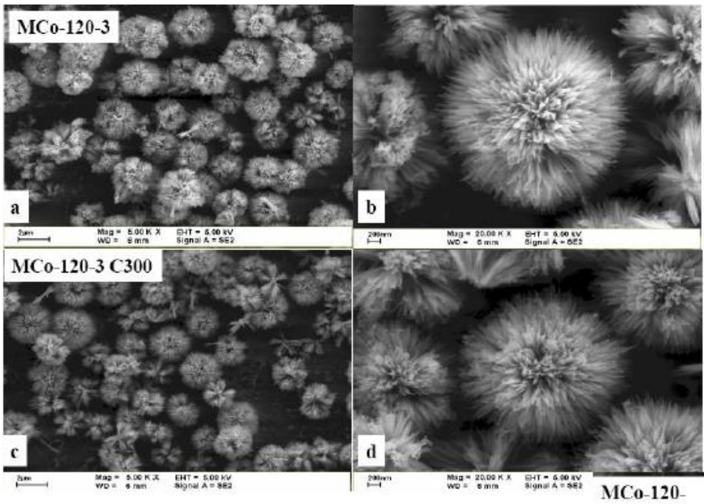

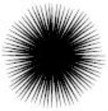

Nanourchins

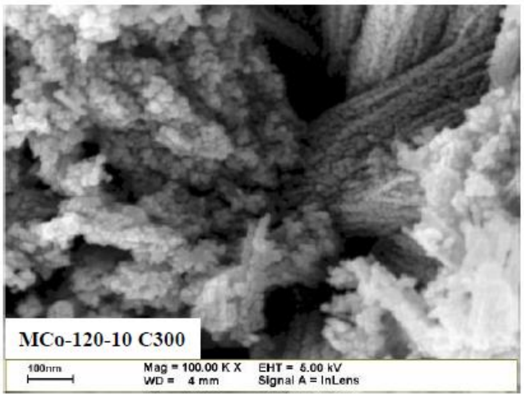

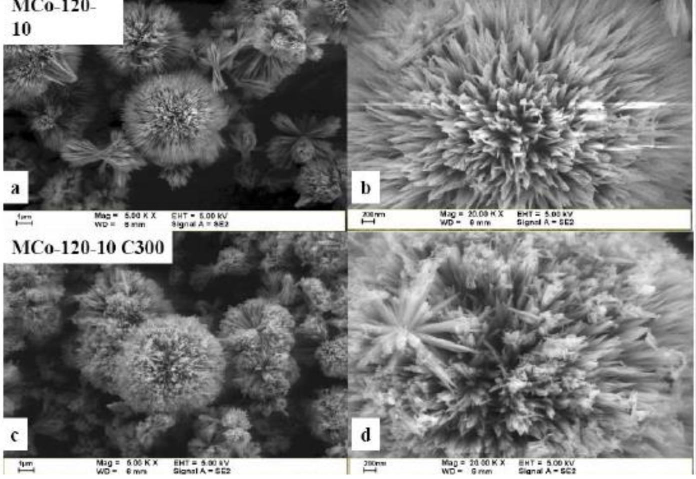

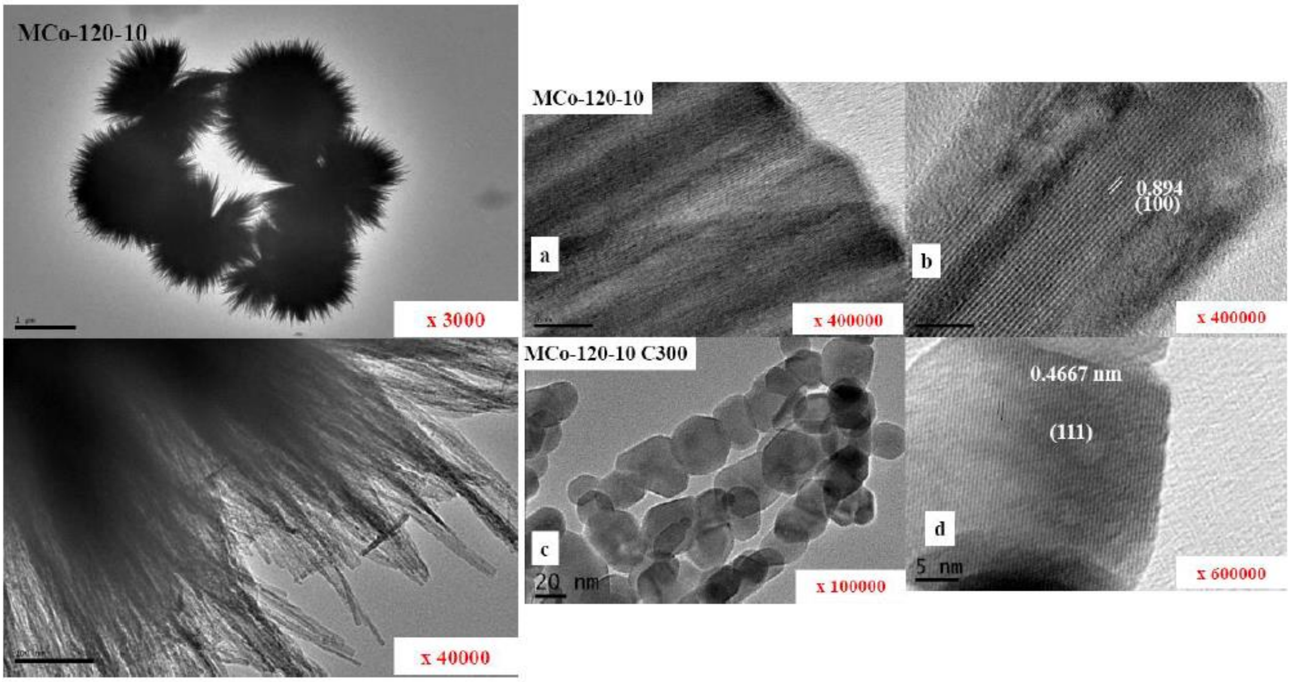
MCo-120-10
x 3000
x 40000
MCo-120-10
a
x 400000
b
0.894
(100)
x 400000
MCo-120-10 C300
c
20 nm
x 100000
0.4667 nm
(111)
d
5 nm
x 600000

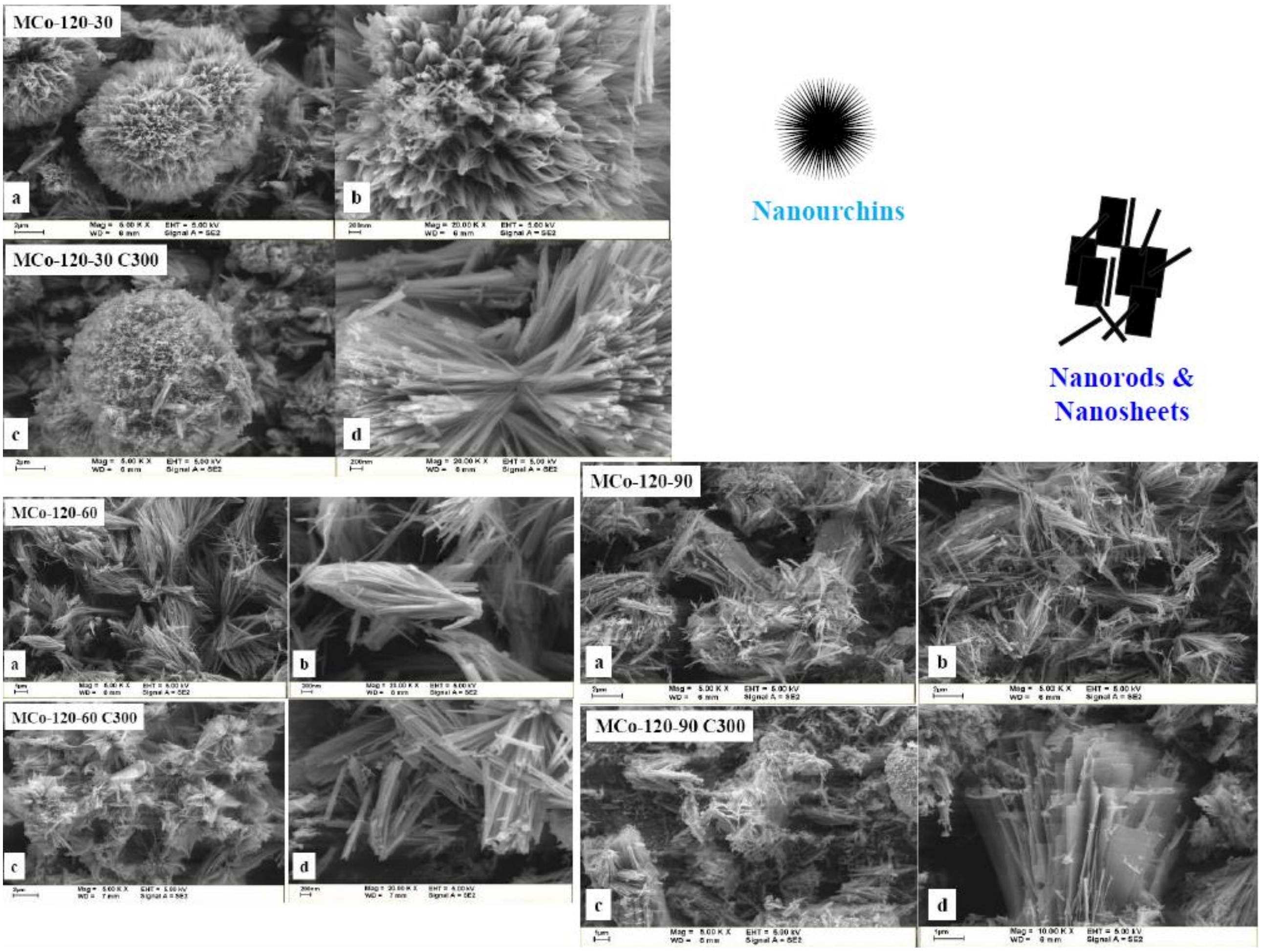
MCo-120-30
a
b
MCo-120-30 C300
c
d
Nanourchins
Nanorods &
Nanosheets
MCo-120-60
a
b
MCo-120-60 C300
c
d
MCo-120-90
a
b
MCo-120-90 C300
c
d

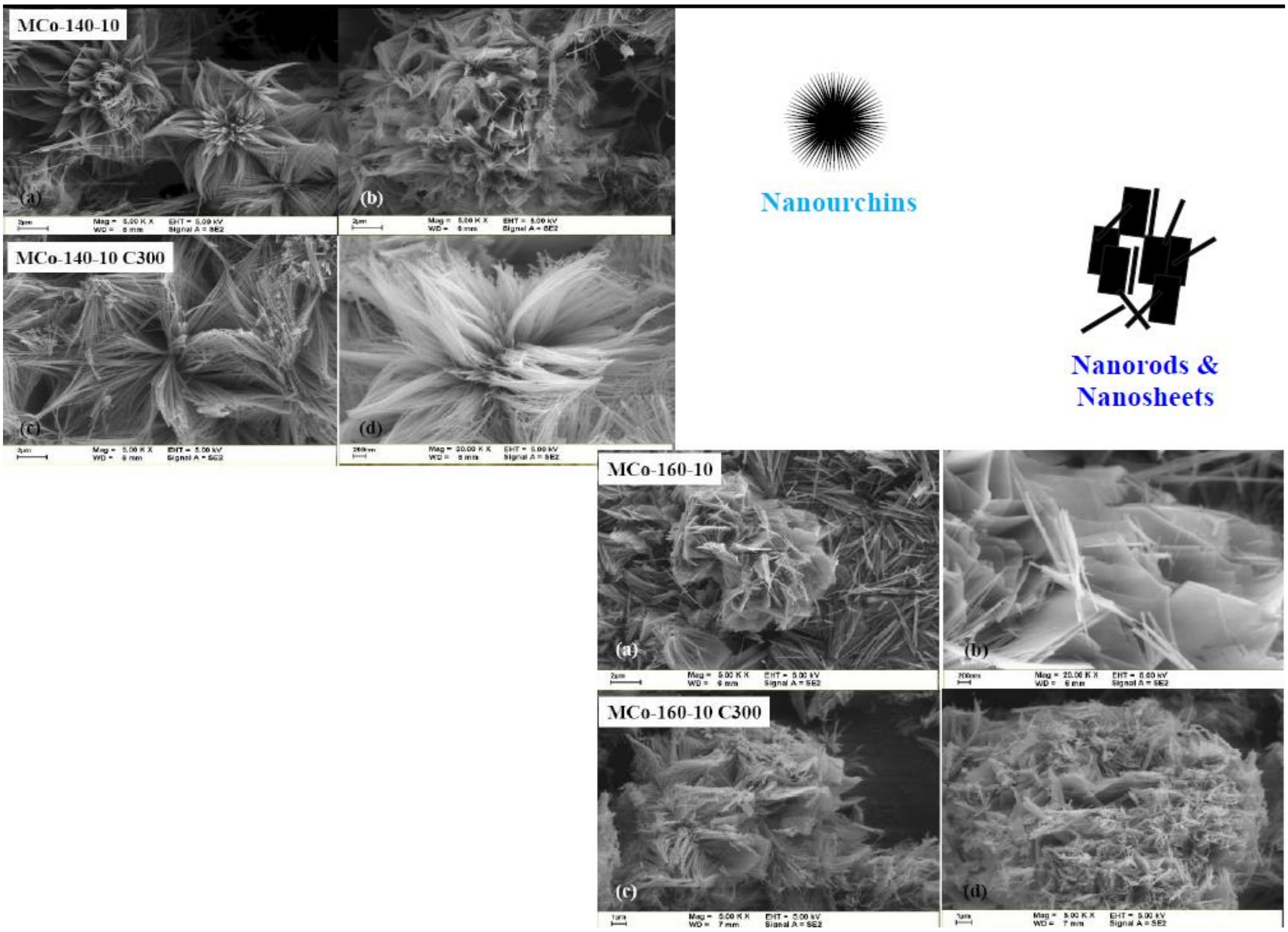
MCo-140-10
(a)
(b)
MCo-140-10 C300
(c)
(d)
Nanourchins
Nanorods &
Nanosheets
MCo-160-10
(a)
(b)
MCo-160-10 C300
(c)
(d)

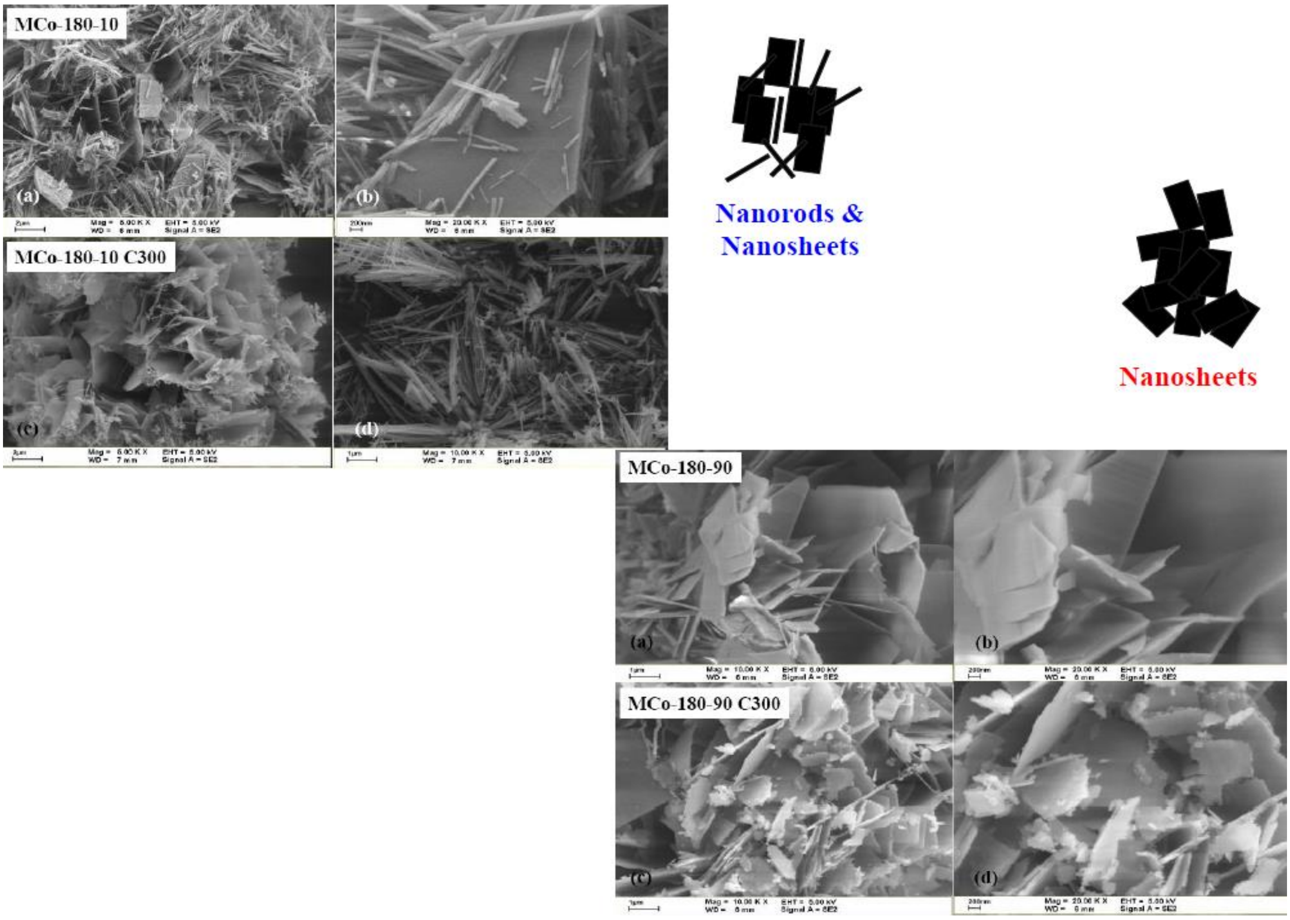
MCo-180-10
(a)
(b)
MCo-180-10 C300
(c)
(d)
Nanorods &
Nanosheets
Nanosheets
MCo-180-90
(a)
(b)
MCo-180-90 C300
(c)
(d)

Catalytic Performance: CO Oxidation

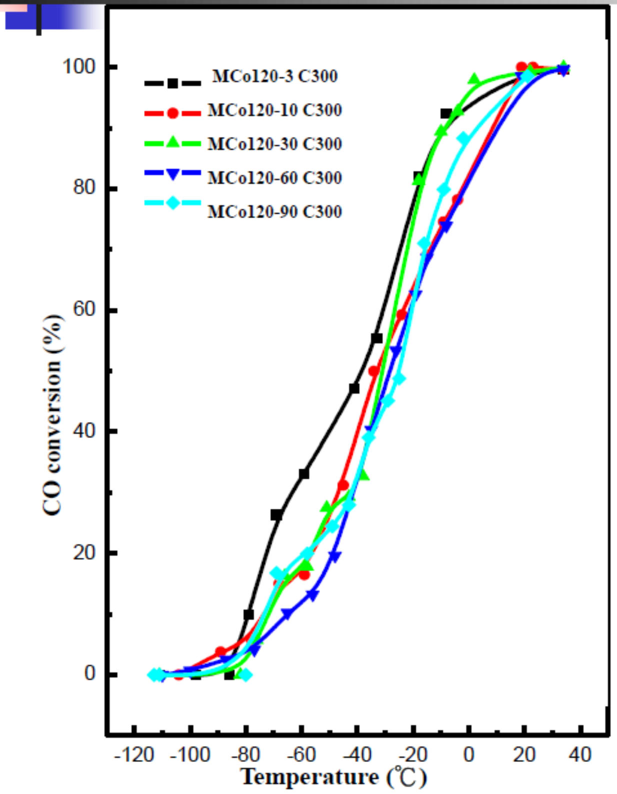

Sample	T_{50} (℃)
MCo120-3 C300	- 38
MCo120-10 C300	- 33
MCo120-30 C300	- 31
MCo120-60 C300	- 28
MCo120-90 C300	- 24

Catalytic Performance: CO Oxidation

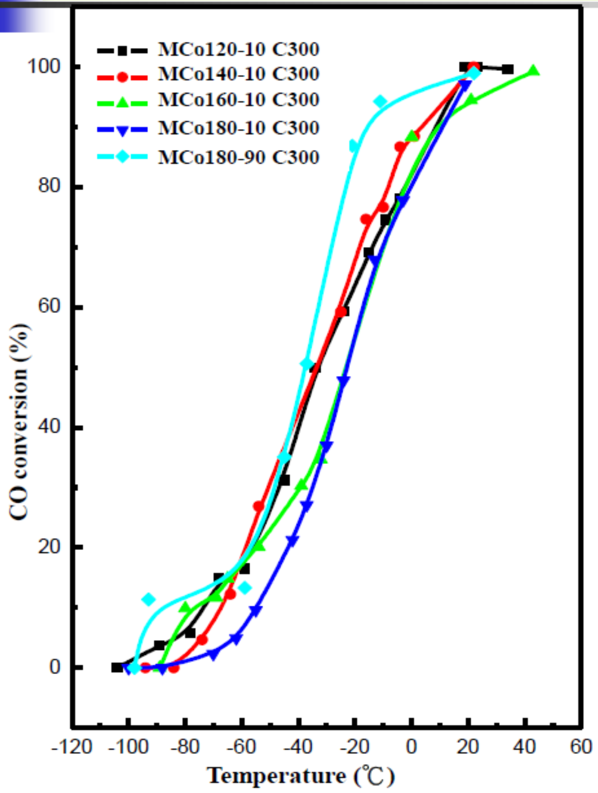

Sample	T_{50} (℃)
MCo120-10 C300	- 33
MCo140-10 C300	- 33
MCo160-10 C300	- 22
MCo180-10 C300	- 22
MCo180-90 C300	- 37

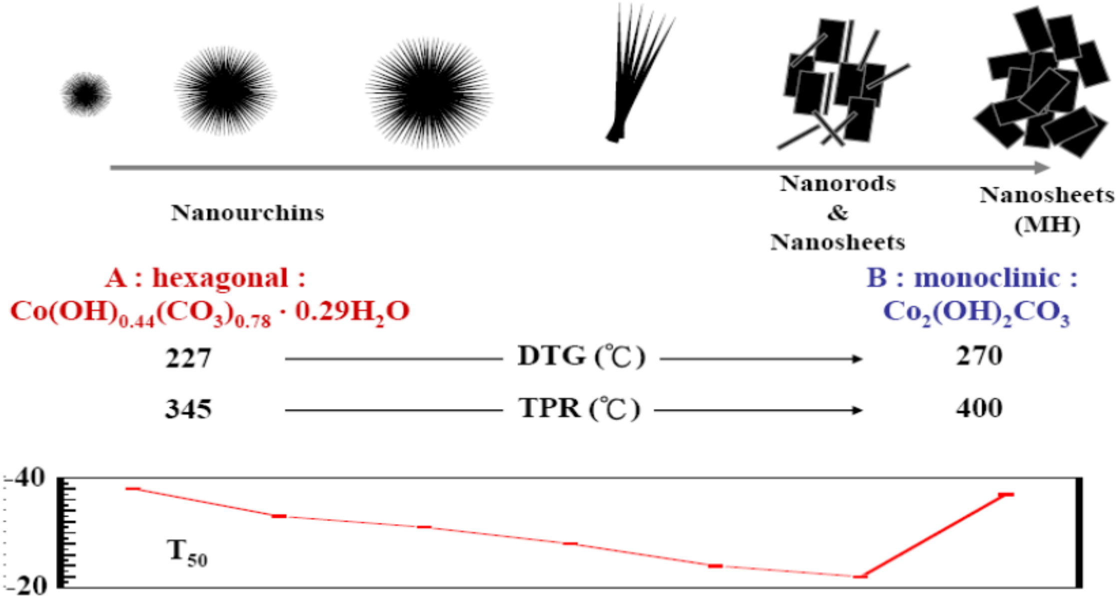

A : hexagonal : $Co(OH)_{0.44}(CO_3)_{0.78} \cdot 0.29H_2O$

B : monoclinic : $Co_2(OH)_2CO_3$

227 —— DTG (℃) → 270

345 —— TPR (℃) → 400

Relationship of nanostructured cobalt oxides on the catalytic performance

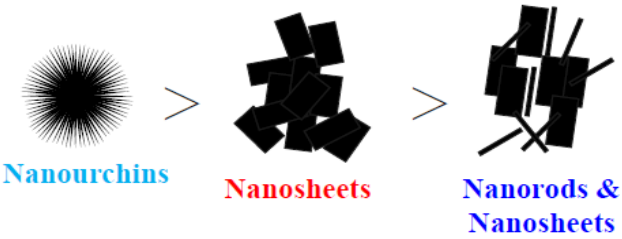

Acknowledgments

Professor Chuin-Tih Yeh (Yuan Ze University)

Professor Shu-Hua Chien (Academia Sinica)

Yu-Hsung Huang **Tsann-Yan Leu** **Ruo-Jiung Yu**

Kuan-Hung Lin **Jia-Lin Bi** **Jin-Yi Shinng**

Supported by Ministry of Science and Technology

作者發表之論文(二)

Evaluation of CO Oxidation over Co_3O_4-supported NiO Catalysts

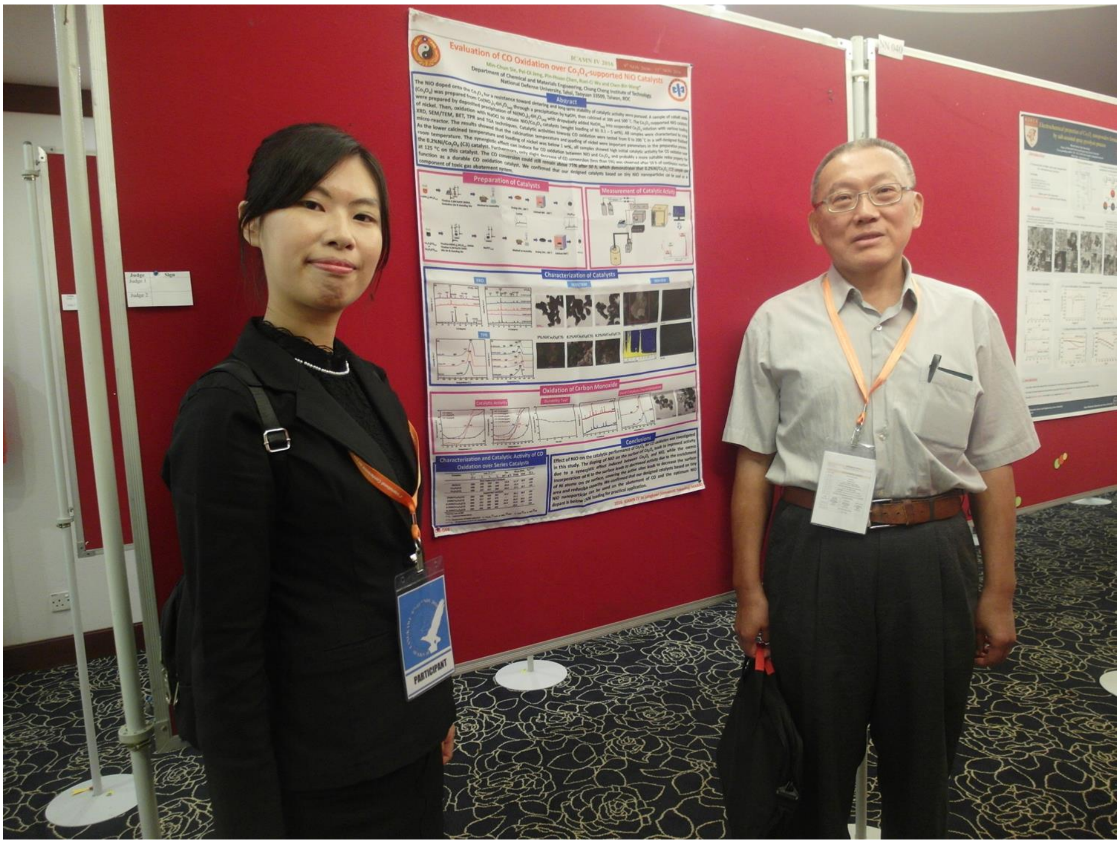

Evaluation of CO Oxidation over Co_3O_4-supported NiO Catalysts

Min-Chun Sie[1, a)], Pei-Di Jeng[1, b)], Pin-Hsuan Chen[1, c)], Ruei-Ci Wu[1, d)] and Chen-Bin Wang[1, e)]

[1]*Department of Chemical and Materials Engineering, Chung Cheng Institute of Technology, National Defense University, Taoyuan, 33509, Taiwan, ROC*

[a)]yikj200@gmail.com
[b)]b9350353@gmail.com
[c)]cbhsmile@gmail.com
[d)]richard82801@yahoo.com.tw
[e)]Corresponding author: chenbinwang@gmail.com

Abstract. The process of doping NiO onto Co_3O_4 for achieving resistance to sintering and obtaining long-term stability of catalytic activity was examined herein. A sample of cobalt oxide (Co_3O_4) was prepared from $Co(NO_3)_2{\cdot}6H_2O_{(aq)}$ via precipitation by NaOH, and then calcined at 300 and 500 ℃. The Co_3O_4-supported NiO catalysts were prepared by deposited precipitation of $Ni(NO_3)_2{\cdot}6H_2O_{(aq)}$ with $NaOH_{(aq)}$ added in a dropwise manner into the suspended Co_3O_4 solution with various loading of nickel. Then, oxidation with NaOCl was employed to obtain NiO/Co_3O_4 catalysts (weight loading of Ni: 0.1 ~ 5 wt%). All of the samples were characterized by using XRD, SEM/TEM, BET, TPR and TGA techniques. Catalytic activities related to CO oxidation were tested from 0 to 200 ℃ in a self-designed fluidized micro-reactor. The results showed that the calcination temperature and loading of nickel were important parameters in the preparation process. With the lower calcined temperature and loading of nickel below 1 wt%, all the samples showed high initial catalytic activity for CO oxidation near room temperature. The synergistic effect can induce CO oxidation between NiO and Co_3O_4, and probably constitute a more suitable redox property for the 0.2%Ni/Co_3O_4 (C3) catalyst. Furthermore, only a slight decrease of CO conversion (less than 5%) was observed after 50 h of continuous reaction under 125 °C on this catalyst. The CO conversion could still remain above 75% after 50 h, which demonstrates that the 0.2%Ni/Co_3O_4 (C3) sample can function as a durable CO oxidation catalyst. We confirmed that our designed catalysts, based on tiny NiO nanoparticles, can be used as a component of a toxic gas abatement system.

Introduction

Carbon monoxide (CO) emissions from stationary industrial processes and mobile automobiles are considered as the main harmful component in polluting the environment. To design novel catalysts for low temperature catalytic oxidation of CO to CO_2 is a promising route to cleaning the air and lowering automotive emissions [1, 2]. This topic suggests extensive applications in numerous fields, such as vehicle exhaust catalysts [3], mine rescue devices [4] and catalytic combustion [5]. From the viewpoint of catalysis, the core problem is to find catalysts that operate efficiently in the CO removal reaction. Many studies have aimed to develop highly active catalysts for CO oxidation based on metal oxides and metal-supported oxides. Highly active and stable Pt-group catalysts for CO oxidation are well known [6-8]. However, besides Au nanoparticles, Pt-group catalysts only show activity for CO oxidation when the reaction temperature exceeds 150 – 200 ℃ [9, 10]. Transition metal-based catalysts have also been developed for CO oxidation due to their low cost and availability [11, 12]. Among the transition metal oxides, cobalt oxide (Co_3O_4) [13, 14] and manganese oxides in various forms (MnO, Mn_2O_3, MnO_2, Mn_3O_4) [15, 16] are particularly attractive material in relation to CO oxidation due to their redox ability of mobile oxygen on the surface. The activity of Co_3O_4 toward oxidation is highly probably because of the relative weakness of the Co-O bond strength of Co3O4, which easily releases reactive oxygen species from the lattice structure.

The rate of CO oxidation over Ni-based catalysts at room temperature has been demonstrated to be very high in studies using single crystal-based model systems under an ultrahigh vacuum (UHV) [17, 18]. Meanwhile, NiO also exhibits an active phase for CO oxidation when deposited on specific supports [19, 20]. However, CO oxidation of supported Ni catalysts under atmospheric pressure conditions has rarely been studied. In this work, we synthesized NiO nanoparticles supported on Co_3O_4 using deposited precipitation and oxidation, and studied their catalytic behavior with regard to CO oxidation from 0 to 200 ℃ under atmospheric pressure. In particular, we focused on the influence of calcination temperature and loading of nickel on Co3O4, as well as their catalytic activity in room temperature CO oxidation. The series of catalysts is characterized by XRD, TEM/SEM, BET, FTIR and TPR. The results of the characterization and the catalytic activity are discussed in relation to the performance of the NiO/Co3O4 catalysts.

Experimental

Preparation of catalysts

Both the NiO and Co_3O_4 catalysts were prepared by precipitation-oxidation method according to previous reports [21, 22], and a series of NiO/Co_3O_4 catalysts with various loading of nickel was fabricated using the deposited precipitation and oxidation method. The precursors were $Ni(NO_3)_2 \cdot 6H_2O$ and $Co(NO_3)_2 \cdot 6H_2O$, the precipitant was NaOH and the oxidant was NaOCl. A sample of Co_3O_4 was prepared from $Co(NO_3)_2 \cdot 6H_2O_{(aq)}$ via precipitation by NaOH, and then calcined at 300 and 500℃. The Co_3O_4-supported NiO catalysts were prepared by deposited precipitation of $Ni(NO_3)_2 \cdot 6H_2O_{(aq)}$ with $NaOH_{(aq)}$ added in a dropwise manner into the suspended Co_3O_4 solution with various loading of nickel. Then, oxidation with NaOCl was employed to obtain NiO/Co_3O_4 catalysts (weight loading of Ni: 0.1 ~ 5 wt%).

Characterization of catalysts

X-ray diffraction (XRD) measurements were made using a Siemens D5000 diffractometer with Cu $K\alpha_1$ radiation (λ = 1.5405 Å) at 40 kV and 30 mA, with a scanning speed in 2θ of $2° \cdot min^{-1}$. The crystallite sizes of cobaltic oxide and nickel oxide were calculated by the Scherrer equation. The surface areas were measured based on the Brunauer–Emmett–Teller (BET) method in the relative pressure range of 0.05 - 0.3, determined from the adsorption branch of nitrogen physisorption isotherms at − 196 ℃. The morphological image and elemental distribution in a cutting plane of the as-prepared NiO/Co_3O_4 was obtained by scanning electron microscopy (SEM, JEOL, JSM-7100F) combined with energy dispersive spectroscopy (EDS). The size of the NiO particles on the surface of the sample was analyzed by transmission electron microscopy (TEM, Hitachi H600-3 a 200kV; HRTEM-JEOL JEM 2011). The reduction behavior of the catalysts was studied using temperature-programmed reduction (TPR) via connection to a thermal conductivity detector (TCD). Approximately 25 mg of the catalyst were heated in a flowing 10% H_2/N_2 gas mixture at a flow rate 10 $ml \cdot min^{-1}$. During TPR, the temperature was programmed to rise at $10°C \cdot min^{-1}$ by using a PID controller from room temperature to 500 °C.

Measurement of Catalytic Activity

The catalytic activities of NiO, Co_3O_4 and NiO/Co_3O_4 catalysts in the oxidation of CO were measured in a self-designed fluidized micro-reactor. A mixture of 0.5% CO, 5.5% O_2 and He as balance reaction gas was fed into a 0.1 g catalyst reactor and the total flow was kept at a rate of 20 $ml \cdot min^{-1}$ during the reaction. Steady-state catalytic activity was measured at each temperature, as the reaction temperature was increased from room temperature to 200 °C in steps of 25 °C. The effluent gas stream was analyzed by using gas chromatography with a thermal conductivity detector (TCD).

Results and Discussion

Characterization of catalysts

The 6th column of Table 1 presents the BET specific surface area of the NiO, Co_3O_4 and NiO/Co_3O_4 catalysts. Both Co_3O_4 (C3) and 0.2%Ni/Co_3O_4 (C3) catalysts possess a large surface area (approaches 30 $m^2 \cdot g^{-1}$) among these catalysts (below 20 $m^2 \cdot g^{-1}$). A comparison of Co_3O_4 (C3) (calcined at 300 °C) with Co_3O_4 (C5) (calcined at 500 °C) shows that the increase in calcined temperature induces the decrease of surface area. The induced decrease due to the thermal treatment might be attributed to grain growth of the particles of cobaltic oxide [23]. In fact, an XRD investigation indicates that the rising calcined temperature of the as-prepared catalyst affects an increase in the degree of crystallinity and particle size of the phase (see the 7th column of Table 1), i.e. 12.5 nm and 17 nm for Co_3O_4 (C3) and Co_3O_4 (C5), 19.3 nm and 26.3 nm for 0.2%Ni/Co_3O_4 (C3) and 0.2%Ni/Co_3O_4 (C5), respectively. Figure 1 presents the XRD patterns of NiO, Co_3O_4 and NiO/Co_3O_4 catalysts. The diffraction pattern of NiO shows the cubic crystal structure at ca. 37.3°, 43.3° and 62.9°, corresponding to (111), (200) and (220) planes, respectively. The obtained diffraction peak of Co_3O_4 shows a well-crystallized phase with a spinel structure [Fig. 1(a)]. In observing the width of the diffraction peaks, the broadening of the peaks can demonstrate the nanocrystalline character of the Co_3O_4 phase. It shows that the Co_3O_4 (C5) diffraction peaks are narrow and sharper than Co_3O_4 (C3), indicating a larger crystal size of Co_3O_4 (C5). The diffraction peaks of series NiO/Co_3O_4 catalysts [Fig. 1(b)] mainly index a spinel structure Co_3O_4 phase; the signal of NiO is not observed in all the samples. The crystallite size of supported NiO is not calculated since the peak intensity is not observed or weak; thus, big errors would result when calculated by the Scherrer equation. This indicates that the doped Ni^{2+} may be incorporated into the Co_3O_4 lattice and/or well-dispersed.

TABLE 1. Characterization and catalytic activity of CO oxidation over series catalysts

Samples	T_C** (℃)	TPR (℃)*** T_i	T_1	T_2	S_{BET} ($m^2 \cdot g^{-1}$)	dCo_3O_4 (nm) Fresh	Used	T_{50}**** (℃)
Non-Supported Catalysts								
NiO(C5)	500	246	259	341	19.9	17.7*	18.0	>200
Co_3O_4(C3)	300	192	284	348	29.9	12.5	—	122
Co_3O_4(C5)	500	227	317	360	18.4	17.1	23.7	115
Supported Catalysts								
5%Ni/Co_3O_4(C5)	300	260	334	361	19.3	20.1	20.4	183
1%Ni/Co_3O_4(C3)	300	217	337	375	—	21.1	—	113
0.2%Ni/Co_3O_4(C5)	300	235	320	360	15.0	26.3	25.5	122
0.2%Ni/Co_3O_4(C3)	300	213	305	360	30.9	19.3	18.9	104
0.1%Ni/Co_3O_4(C3)	300	206	280	345	—	18.3	—	116

*Particle size of NiO

** T_C：Calcined temperature

***T_i：Temperature of initial reduction T_1：$Co_3O_4 \xrightarrow{[H]} CoO$ or $NiO_X \xrightarrow{[H]} NiO$ T_2：$CoO \xrightarrow{[H]} Co$ or $NiO \xrightarrow{[H]} Ni$

**** T_{50}：Temperature of 50 % CO conversion

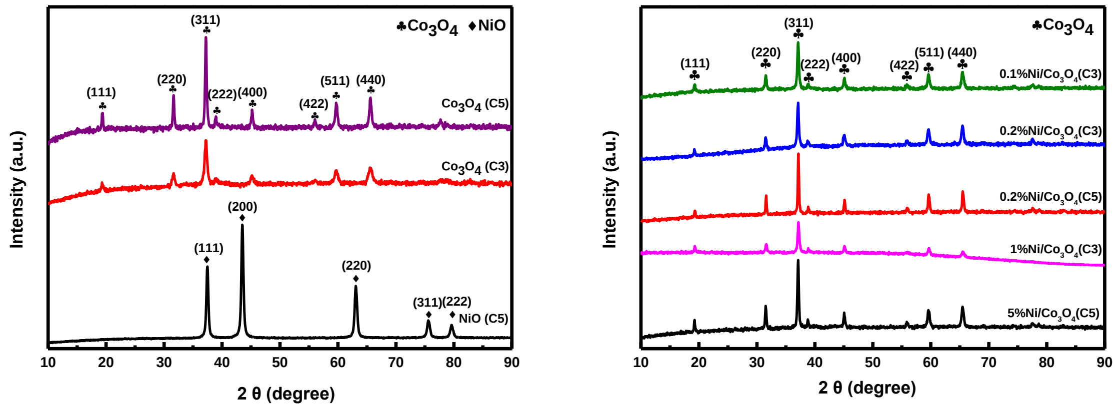

(a) (b)

FIGURE 1. XRD patterns of (a) NiO and Co_3O_4 (b) NiO/Co_3O_4 catalysts

Figure 2 shows the TEM/SEM images of three NiO/Co_3O_4 catalysts. All three exhibit a homogeneous microstructure with packing of spherical particles with grain size ranging from 50 to 100 nm. A layer of white film from the 0.2% loading of Ni and dispersed nanoparticles over the 5% loading of Ni covers the support surface. It is interesting to find that the NiO particles are well dispersed on the surface of Co_3O_4. To verify that NiO is dispersed on the surface of Co_3O_4, an EDS mapping photograph of the 5%Ni/Co_3O_4 (C5) sample was taken on an SEM apparatus. Figure 3 shows the analysis of the SEM-EDS image: the Ni and Co atoms are homogeneously dispersed, confirming the above TEM analysis.

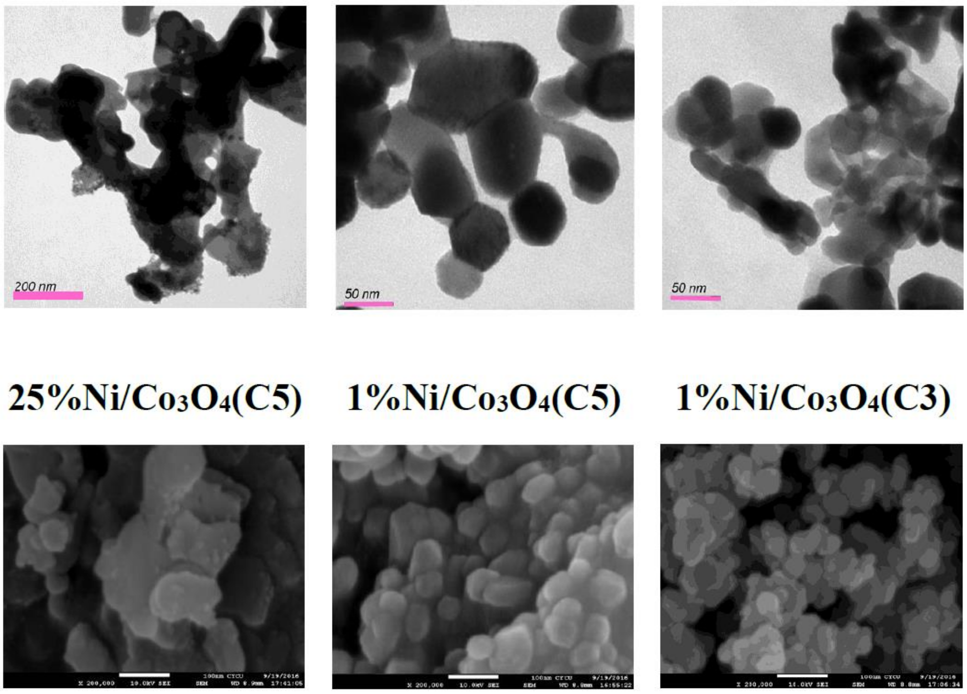

FIGURE 2. TEM/SEM images of NiO/Co_3O_4 catalysts

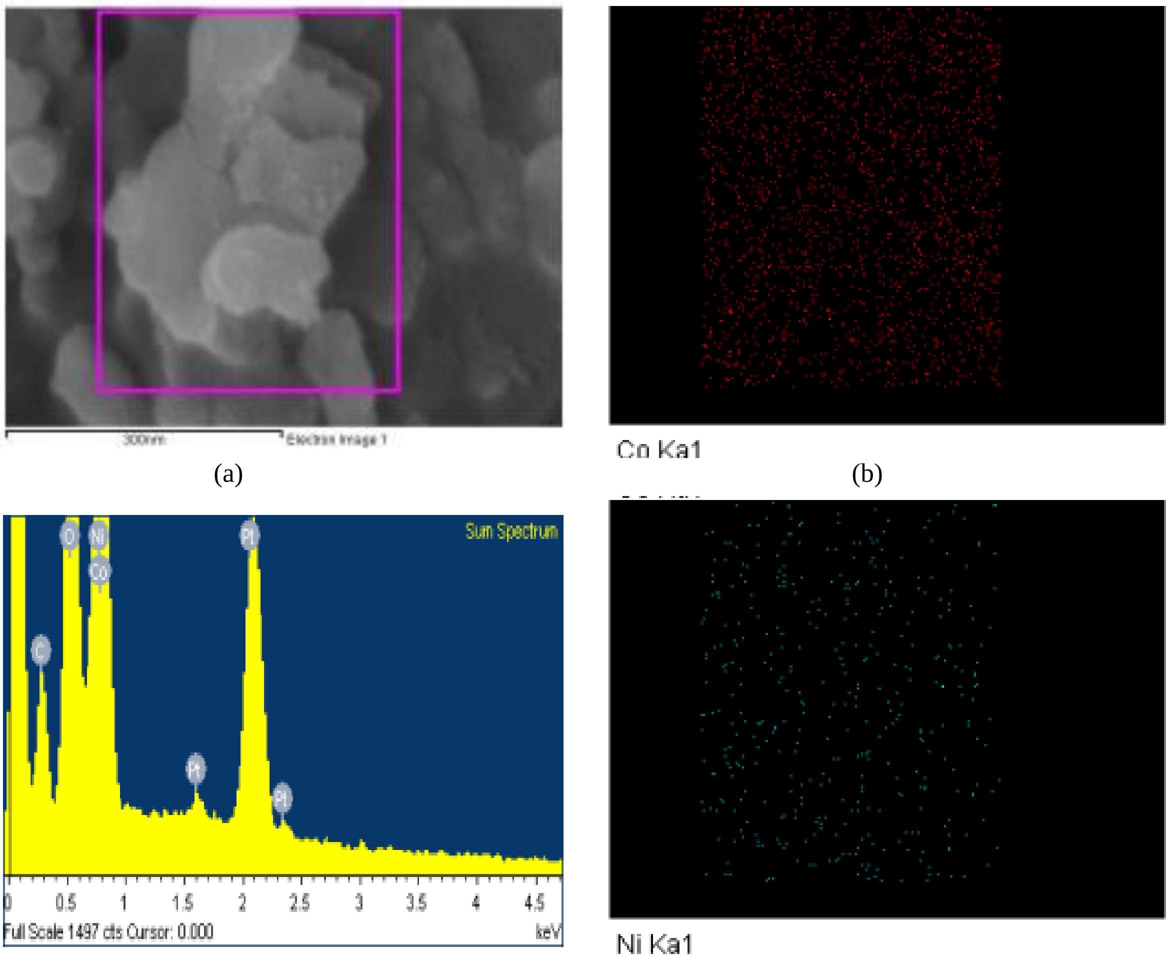

(a) (b)

(d) (c)

FIGURE 3. SEM-EDS images of 5%Ni/Co_3O_4 (C5) catalyst: (a) SEM image (b) Mapping of Co (c) Mapping of Ni (d) EDS spectrum

To understand the M-O (Co or Ni) bond strength in the NiO/Co_3O_4 catalysts, the TPR technique was used to elucidate the reduction behavior of these catalysts. Figure 4 shows the TPR profiles of the prepared series catalysts. The profiles of Fig. 4(b) show one faint peak (T_i) and two sequent reduction peaks (T_1 and T_2). According to the literature, the first two peaks were attributed to the removal of oxygen species adsorbed on oxygen vacancies and the reduction of Co^{3+} to Co^{2+} (or Ni^{3+} to Ni^{2+}), respectively, and the third peak to the reduction of Co^{2+} to Co metal (or Ni^{2+} to Ni metal) [24]. For comparison, the reduction profile of pure NiO and Co_3O_4 [Fig. 4(a)] was also conducted, showing a big peak around 300 – 400 °C due to the reduction of NiO to Ni metal, and CoO to Co metal as observed elsewhere [25]. The 3rd to 5th columns of Table 1 present the reduction temperatures (T_i, T_1 and T_2) of series catalysts. The addition of Ni atoms, supported on the surface on the framework of Co_3O_4, led to a decrease in the reduction temperature of T_i with the decreasing loading of Ni, i.e. 260, 217, 213 and 206 °C for 5%Ni/Co_3O_4 (C5), 1%Ni/Co_3O_4 (C3), 0.2%Ni/Co_3O_4 (C3) and 0.1%Ni/Co_3O_4 (C3), respectively, due to the increase of its reducible capacity. Comparing the effect of surface area with the reduction behavior reveals an apparent shift of T_i to a lower temperature with the increase of surface area. We inferred that the reduction temperature of T_i should be the crucial factor influencing the CO oxidation activity.

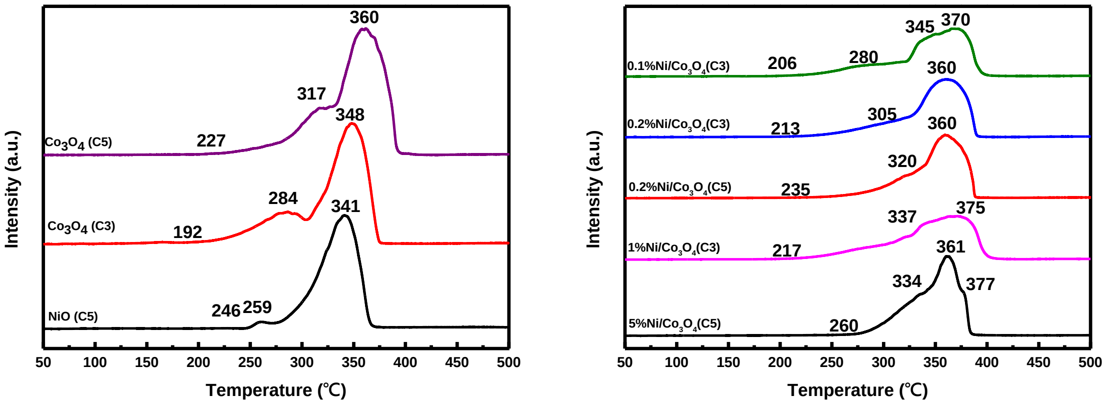

(a) (b)

FIGURE 4. TPR profiles of (a) NiO and Co_3O_4 (b) NiO/Co_3O_4 catalysts

Oxidation of Carbon Monoxide

Figure 5 displays the CO oxidation activity obtained from the samples, showing that CO conversion increases with increased reaction temperature; the activity is in order of NiO < 5%Ni/Co_3O_4 (C5) < Co_3O_4 < 1%Ni/Co_3O_4 (C3) < 0.2%Ni/Co_3O_4 (C3). Pure NiO is less active for CO oxidation [Fig. 5(a)] so that the needed temperature exceeds 200 °C, but it can significantly improve the activity when supported on the Co_3O_4 surface [Fig. 5(b)], indicating that the presence of NiO alters the surface properties of Co_3O_4 and promotes its CO oxidation ability. To exclude the high activity of Co_3O_4 [Fig. 5(a)], a series comparative catalysts, NiO/Co_3O_4 [Fig. 5(b)], suggests that the enhanced activity obtained from the Co_3O_4-supported catalysts is not due to the dispersed NiO particles, but rather to a synergistic effect induced between Co_3O_4 and NiO. The synergistic effect between perovskite and metal oxides for CO oxidation has been found for an $LaCoO_3$–Co_3O_4 system in a previous work [26]. The synergistic effect can induce CO oxidation between NiO and Co_3O_4, and probably a more suitable redox property for 0.2%Ni/Co_3O_4 (C3) catalyst. The T_{50} (temperature at 50% CO conversion, list in the last column of Table 1) of the 0.2%Ni/Co_3O_4 (C3) catalyst occurs at 104 °C, which is lower than that of the other catalysts: the T_{50} values for the 1%Ni/Co_3O_4 (C3), Co_3O_4 and 5%Ni/Co_3O_4 (C5) catalysts are 113, 122 and 183 °C, respectively. The effect of NiO loading on the activity of series NiO/Co_3O_4 catalysts is due to the relationship of Ni. A significant increase in the activity can be observed for the decreased loading of Ni, demonstrating that the presence of NiO is crucial to the reaction. The reason is that the less loading of Ni at the beginning increases the synergistic effect by improving the contact area with Co_3O_4 and reducible capacity, but the excess presence of Ni decreases the catalytic performance due to the enrichment of Ni atoms on the surface; covering the active sites leads to a decrease in the surface area and reducible capacity. In comparison, the optimum NiO dopant is below 1%Ni loading.

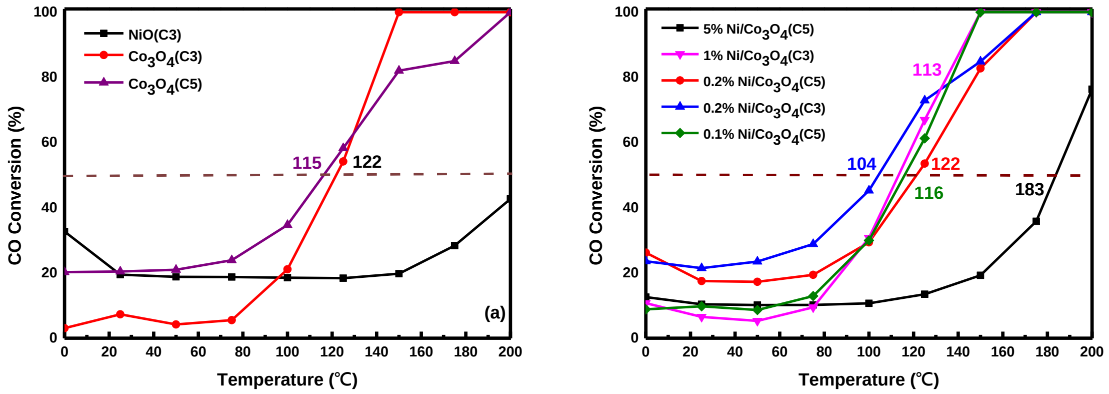

(a) (b)

FIGURE 5. Catalytic activities of (a) NiO and Co_3O_4 (b) NiO/Co_3O_4 catalysts toward CO oxidation as a function of temperature

Besides activity, the stability of catalyst is another important factor for CO oxidation [27, 28]. Figure 6 shows the stability test of 0.2%Ni/Co_3O_4 (C3) catalyst at 125 °C. The stability test result shows that the catalyst can maintain catalytic activity for 50 h. Furthermore, only a little decrease of CO conversion (less than 5%) was observed after 50 h of continuous reaction at 125 °C. The CO conversion could still remain above 75% after 50 h, which demonstrates that the 0.2%Ni/Co_3O_4 (C3) sample can function as a durable CO oxidation catalyst. The deactivation of the catalyst can be attributed to the following reasons. First, moisture could compete with reactants to occupy some active sites and thus reduce the reaction rate. Second, the surface reconstruction and/or sintering of the catalyst would lower the catalytic activity during CO oxidation [29]. Slight variations were found in the XRD patterns and TPR profiles when comparing the fresh and used 0.2%Ni/Co_3O_4 (C3) catalyst. XRD analysis [Fig. 7(a)] reveals that the catalytic test led to no change in the phase and crystallinity of the cobalt oxide domains. The relative intensity of the XRD peaks is similar for the fresh and used samples, and the particle size approaches 19 nm (see the 7th and 8th columns of Table 1). The reduction behavior of the fresh and spent samples is shown in Figure 7(b). The main reduction peak indicates the reduction of cobalt oxide. A slight shift of the reduction peak for the spent catalyst demonstrates that the surface reconstruction may occur, with easy reduction to maintain the catalytic performance.

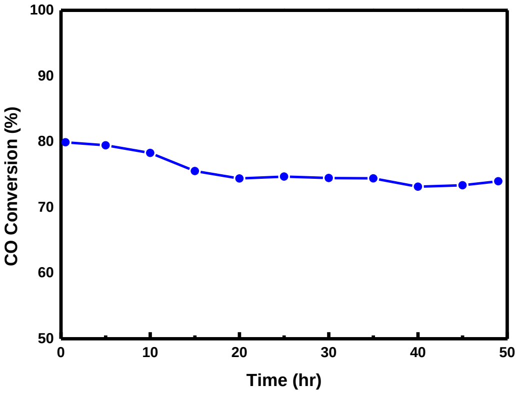

FIGURE 6. Stability test of 0.2%Ni/Co_3O_4 (C3) catalyst at 125 °C

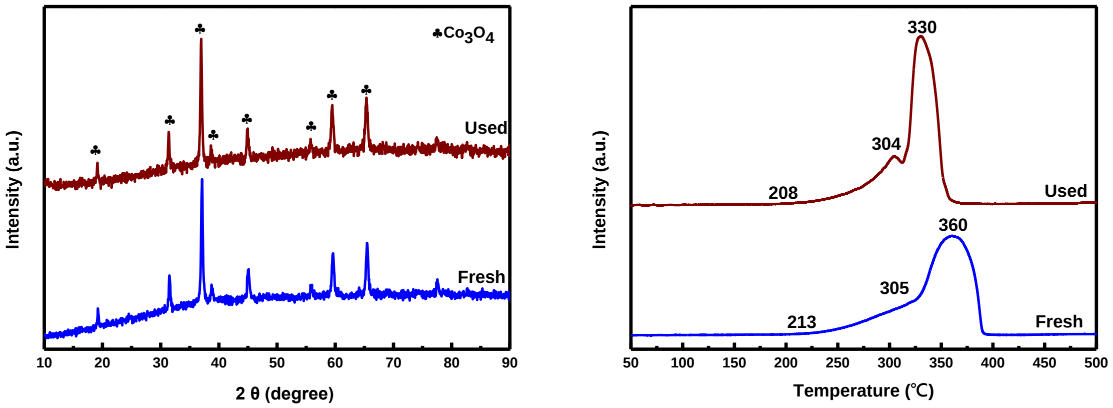

(a) (b)

FIGURE 7. Characterization of fresh and used 0.2%Ni/Co_3O_4 (C3) catalysts: (a) XRD patterns (b) TPR profiles

Conclusions

The effect of NiO on the catalytic performance of Co_3O_4 for CO oxidation was investigated in this study. The doping of NiO on the surface of Co_3O_4 leads to improved activity due to a synergistic effect induced between Co_3O_4 and NiO, while the excess incorporation of Ni to the surface leads to decreased activity due to the enrichment of Ni atoms on the surface, and covering the active sites leads to decreased surface area and reducible capacity. We confirmed that our designed catalysts based on tiny NiO nanoparticles can be used for the abatement of CO, and that the optimum NiO dopant is below 1%Ni loading for practical applications.

Acknowledgements

We are pleased to acknowledge the financial support for this study from the Ministry of Science and Technology of the Republic of China under contract number of MOST 105-2119-M-606-001-.

References

1. S. Royer and D. Duprez, ChemCatChem **3**, 24-65 (2011).
2. S. Li, H. Zhu, Z. Qin, G. Wang, Y. Zhang, Z. Wu, Z. Li, G. Chen, W. Dong and Z. Wu, Appl. Catal. B: Environmental **144**, 498-506 (2014).
3. R. K. Usmen, G. W. Graham, W. L. H. Watkins and R. W. McCabe, Catal. Letters **30**, 53-63 (1994).
4. A. B. Lamb, W. C. Bray and J. C. W. Fraser, Ind. Eng. Chem. **12**, 213-221 (1920).
5. D. L. Trimm, Appl. Catalysis **7**, 249-282 (1983).
6. S. D. Gardner, G. B. Hoflund, B. T. Upchurch, D. R. Schryer, E. J. Kielin and J. Schryer, J. Catalysis **129**, 114-120 (1991).
7. L. Liu, F. Zhou, L. Wang, X. Qi, F. Shi and Y. Deng, J. Catalysis **274**, 1-10 (2010).
8. K. An, S. Alayoglu, N. Musselwhite, S. Plamthottam, G. Melaet, A. E. Lindeman and G. A. Somorjai, J. Am. Chem. Soc. **135**, 16689-16696 (2013).
9. C. T. Campbell, Science **306**, 234-235 (2004).
10. M. Shen, L. Lv, J. Wang, J. Zhu, Y. Huang and J. Wang, Chem. Eng. J. **255**, 40-48 (2014).
11. G. Glaspell, H. M. Hassan, A. Elzatahry, V. Abdalsayed and M. S. El-Shall, Top. Catalysis **47**, 22-31 (2008).
12. J. Xu, Y. Q. Deng, X. M. Zhang, Y. Luo, W. Mao, X. J. Yang, L. Ouyang, P. Tian and Y. F. Han, ACS Catalysis **4**, 4106-4115 (2014).
13. J. Jansson, A. E. C. Palmqvist, E. Fridell, M. Skoglundh, L. O. Sterlund, P. Thormahlen and V. Langer, J. Catalysis **211**, 387-397 (2002).
14. C. B. Wang, C. W. Tang, S. J. Gau and S. H. Chien, Catal. Letters **101**, 59-63 (2005).
15. S. Liang, F. Teng, G. Bulgan, R. Zong and Y. Zhu, J. Phys. Chem. C **112**, 5307-5315 (2008).
16. L. C. Wang, L. He, Y. M. Liu, Y. Cao, H. Y. He, K. N. Fan and J. H. Zhuang, J. Catalysis **264**, 145-153 (2009).
17. J. Knudsen, L. R. Merte, G. Peng, R. T. Vang, A. Resta, E. Laegsgaard, J. N. Andersen, M. Mavrikakis and F. Besenbacher, ACS Nano. **4**, 4380-4387 (2010).
18. G. Peng, L. R. Merte, J. Knudsen, R. T. Vang, E. Laegsgaard, F. Besenbacher and M. Mavrikakis, J. Phys. Chem. C **114**, 21579-21584 (2010).
19. S. W. Han, D. H. Kim, M. G. Jeong, K. J. Park and Y. D. Kim, Chem. Eng. J. **283**, 992-998 (2015).
20. Z. Chen, Y. L. Xie, J. X. Qiu and Z. H. Chen, Adv. Mater. Research **842**, 237-241 (2014).
21. T. L. Lai, C. C. Lee, K. S. Wu, Y. Y. Shu and C. B. Wang, Appl. Catal. B: Environmental **68**, 147-153 (2006).
22. H. K. Lin, H. C. Chiu, H. C. Tsai, S. H. Chien and C. B. Wang, Catal. Letters **88**, 169-174 (2003).
23. G. A. El-Shobaky and N. M. Deraz, Mater. Letters **47**, 231-240 (2001).
24. S. Zhong, Y. Sun, H. Xin, C. Yang, L. Chen and X. Li, Chem. Eng. J. **275**, 351-356 (2015).
25. K. Takehira, Catal. Surv. Asia **6**, 19-32 (2002).
26. L. Zhong, F. Hai, P. Xiao, J. Hong and J. Zhu, RSC Adv. **4**, 61476-61481 (2014).
27. K. Liu, A. Wang and T. Zhang, ACS Catalysis **2**, 1165-1178 (2012).
28. X. Xie, Y. Li, Z.Q. Liu, M. Haruta and W. Shen, Nature **458**, 746-749 (2009).
29. S. Vepřek, D. L. Cocke, S. Kehl and H. R. Oswald, J. Catalysis **100**, 250-263 (1986).

作者發表之論文(三)

Graphene Sponge as an Efficient and Recyclable Oil Sorbent

Graphene Sponge as an Efficient and Recyclable Oil Sorbent

Pin-Hsuan Chen[1, a)], Min-Chun Sie[1, b)], Pei-Di Jeng[1, c)], Ruei-Ci Wu[1, d)] and Chen-Bin Wang[1, e)]

[1]*Department of Chemical and Materials Engineering, Chung Cheng Institute of Technology, National Defense University, Taoyuan, 33509, Taiwan, ROC*

a)cbhsmile@gmail.com
b)yikj200@gmail.com
c)b9350353@gmail.com
d)richard82801@yahoo.com.tw
e)Corresponding author: chenbinwang@gmail.com

Abstract. Fructose, an environmentally friendly reducing agent, was chosen during the process of reduction and self-assembly of graphene oxide (r-GO) via the hydrothermal method to prepare the graphene sponge (r-GS). Graphite oxide (GO) was prepared by oxidizing graphite (G) powders through a modified Hummers method. The GO dispersion (10 mg/mL) was mixed with equal mass ratio of fructose and ultrasonic-assisted dispersing in a beaker at RT for 30 min. Then, the suspended solution was transferred to a 200 mL Teflon-lined autoclave and maintained at 160 ℃ for 6 h. After cooling to RT, the black rod was washed with deionized water and lyophilized to obtain r-GS. The samples were characterized by XRD, TEM/SEM, BET, EA, FTIR, Raman and TPR. The absorption capacity and recycling measurement for oil over the fabricated r-GS was evaluated. In the preliminary results, the hydrophobic r-GS showed light weight and formed 3D porous structure that could enhance the absorption of organic solvents and oils. The absorption capacities of r-GS for various organic solvents and oils were quantified. The absorption capacities were in the range of 15 ~ 38 g/g. The ultrahigh absorption capacity indicates that the absorption is more like an accommodation of oils in the hydrophobic micro- and macro- pores of the r-GS. In particular, the absorption capacity for vegetable oil is 37.8 g/g, indicating that the r-GS can be used for oil leakage treatment.

Introduction

In recent years, high molecular materials through assembling of nanomaterials into macroscopic structures, while keeping the unique properties of nanoscale building blocks [1-3], are gaining much attention in its great significance to advance the practical applications, i.e. adsorbents for various pollutants, heavy metals, dyes, organic solvents and nonmetal ions [4-8]. Since the discovery of graphene, it has been extensively investigated as a typical carbon nanostructure. Graphene (r-G), graphene oxide (r-GO), graphite (G) and graphite oxide (GO) have attracted enormous interest in the development of composite materials and catalysts [9-13] due to their remarkable physical, chemical and electrical characteristics, including a very high specific surface area, as well as excellent stabilities [14]. Among these materials, the precursor of r-G and r-GO can be obtained easily by oxidizing expandable graphite powders [15]. Interestingly, both r-G and r-GO exhibit excellent activity due to their privileged lamellar flexible structure with 3D hierarchical porous texture; a wide range of introduced oxygen-containing functional groups, such as epoxy (C-O-C), hydroxyl (OH) and carboxyl (COOH) [16, 17] can overcome hydrophobicity of pristine graphene, thus making r-GO an attractive candidate for the bottom-up assembly of r-G into nacroscale structures. Due to the hydrophobic nature of oils, r-G should be in the reduced form for oil removal; many types of r-G adsorbent have been found in regard to the removal of oil [18-22]. Porous r-G could accommodate more oils; thus, is the main form employed in the oil–water separation. Also, r-G and r-GO supported catalysts have been applied to many kinds of chemical reactions [23-25].

Four types of r-G have been designed for application in the removal of oil. The first is r-GS, widely adopting the hydrothermal method in a preparation that possesses potential adsorption performance in oil adsorption [18, 19]. The second is r-G amended polymer (such as the polyurethane) sponge [22, 26]. The third is r-G amended cotton [27] and fourth is the porous r-G composite with other inorganic materials and/or polymers [28-30]. The preparation of r-GS is easier and more reproducible among these materials. In particular, the hydrothermal reduction of r-GO is regarded as the easiest method to prepare r-GS for oil removal. However, using reducing reagents such as thiourea and ammonia might cause environmental pollution [18, 19]. Therefore, the application of environmentally friendly reducing reagents for the preparation of r-GS has received increased attention. In this paper, an environmentally friendly reducing agent, fructose, has been chosen fot the process of reduction and self-assembly of r-GO via the hydrothermal method to prepare the r-GS, and is characterized with XRD, TEM/SEM, FTIR, Raman and TPR tools. The adsorption and regeneration capacities of oils and organic solvents on r-GS are evaluated.

Experimental

Preparation of r-GS

A modified Hummers method was employed to fabricate GO from natural graphite powder [15]. Briefly, graphite (1 g) was added to concentrated sulfuric acid (46 mL) with stirring under an ice bath, sodium nitrate (0.5 g) was then added, and the mixture was still stirred for 4 h. Under vigorous agitation, potassium permanganate (3 g) was slowly added while the temperature of suspension was kept lower than 20 ℃ under an ice bath. Subsequently, the reaction system was transferred to a 35 ℃ water bath and stirred for about 2 h, forming a thick paste. Then, 46 mL de-ionized water was added, and the solution was stirred for 1 h at 95 ℃. An additional 140 mL of de-ionized water were added, followed by the slow addition of 20 mL of H_2O_2 (20%) till no bubble formed, turning the color of the solution from dark brown to yellow. The mixture was filtered and washed with 200 mL diluted HCl (1:10) solution to remove metal ions, followed by washing with de-ionized water to remove the acid till pH of 7 resulted to obtain GO. Then, dried solid-state, dark brown GO powder (100 mg) was dissolved in de-ionized water (10 ml) and ultrasonicated for 1 h to form a colloidal dispersion of r-GO. Subsequently, an equal mass ratio of fructose solution was added with uniform ultrasonic stirring for 0.5 h. The dispersed r-GO was transferred into a sealed reactor with a Teflon-lined autoclave and maintained under 160 ℃ for 6 h. After slowly cooling to RT, a wet black cylindrical r-GS hydrogel block was obtained. Finally, the r-GS hydrogel block was washed with de-ionized water and lyophilized under – 50 ℃.

Characterization of r-GS

X-ray diffraction (XRD) measurements were made using a Siemens D5000 diffractometer with Cu $K\alpha_1$ radiation (λ = 1.5405 Å) at 40 kV and 30 mA with a scanning speed in 2θ of $2°\cdot min^{-1}$. Fourier transform infrared (FTIR) spectra were recorded using a Nicolet 6700 FI-IR spectrometer (Nicolet). The GO powder was mixed with potassium bromide to form the pellets in order to scan the FTIR spectra. The microstructures and structures on the nanoscale were acquired by scanning electron microscopy (SEM, JEOL, JSM-7100F) and transmission electron microscopy (TEM, Hitachi H600-3 a 200kV; HRTEM - JEOL JEM 2011). Raman spectra were carried out using a Witec Alpha 300R confocal Raman microscope. The excitation wavelength is 532 nm and a laser power of ~ 0.1 mW was chosen in order to avoid laser-induced damage of the r-GS skeleton. The reduction behavior was studied using temperature-programmed reduction (TPR) with connected to a thermal conductivity detector (TCD). Approximately 25 mg of the sample were heated in a flowing 10% H_2/N_2 gas mixture at a flow rate 10 $ml\cdot min^{-1}$. During TPR, the temperature was programmed to rise at 10 $°C\cdot min^{-1}$ by using PID controller from RT to 900 °C.

Oil and organic solvent absorption

We evaluated the adsorption capacity (Q, $g\cdot g^{-1}$) of r-GO for various oils (vegetable oil and machine oil) and organic solvents (ethanol, acetone and cyclohexane). The r-GS was first put into the oils or organic solvents for 10 min (Fig. 1); after picking out, the weights of the r-GO before and after adsorption were measured for Q calculation. The absorption capacity denotes the ratio of the final weight to the initial weight after full absorption. In the recycling of r-GS, upon the adsorption of vegetable oil, the r-GS samples were squeezed and then dried by natural evaporation. Then, with the removal of vegetable oil by burning, the absorbed and dried r-GS was placed in a glass place and fired (Fig. 2).

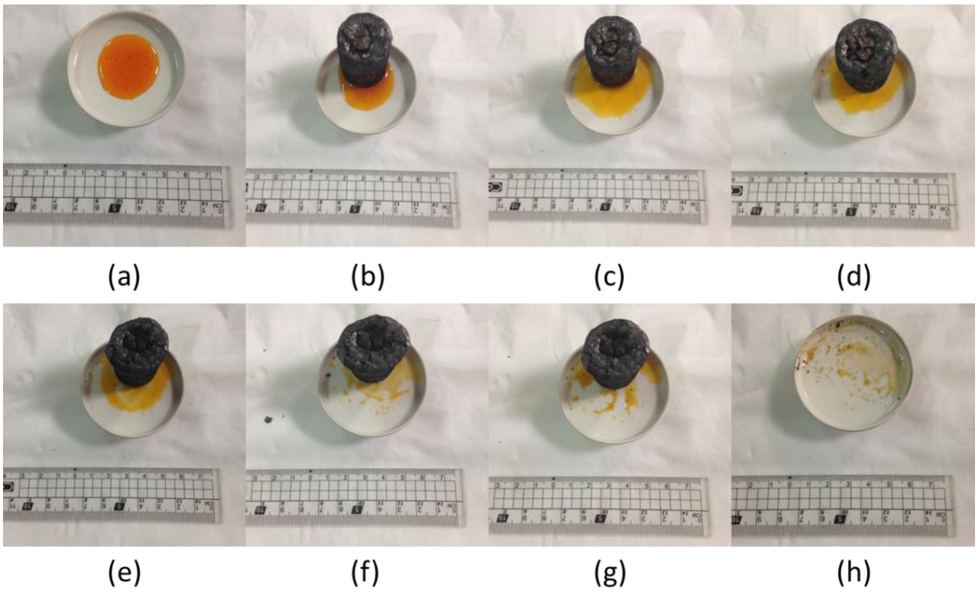
(a) (b) (c) (d)

(e) (f) (g) (h)

FIGURE 1. Absorption of vegetable oil test: vegetable oil was stained by methyl red, and took a picture at interval of 20 s till complete absorption on r-GS.

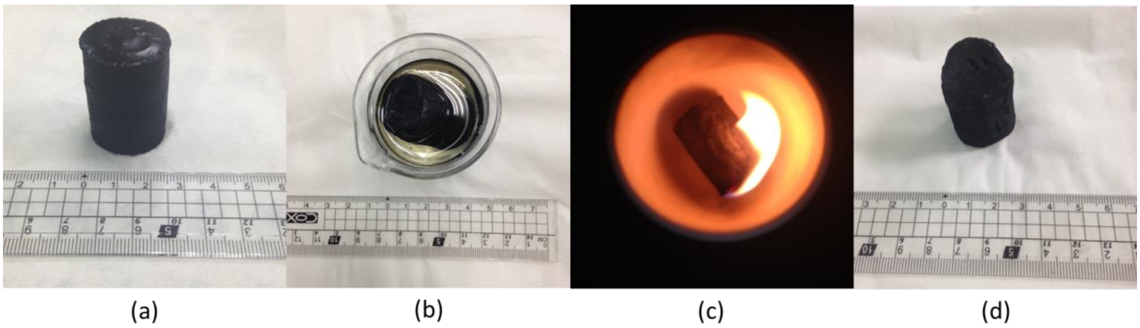

FIGURE 2. Absorption and removal of vegetable oil: (a) Raw r-GS (b) Absorbed vegetable oil (c) During the burning (d) After the burning

Results and Discussion

Characterization of r-GS

Figure 3 presents the XRD patterns of the G, GO, r-GO and r-GS samples. In the XRD patterns, a much narrower peak of G was centered at $2\theta = 26.6°$ (d-spacing 3.36 Å) corresponding to the (002) while the fatter diffraction peak for GO and r-GO appear around $2\theta = 10.3°$ (d-spacing 8.62 Å) and 12.3° (d-spacing 7.21 Å), respectively. This indicates that the interlayer spacing of carbon structure instantaneously increases along with the graphite oxidation. After the reduction and self-assembly of r-GO, and freeze-drying, a new much broadened diffraction peak at $2\theta = 24.5°$ (d-spacing 3.67 Å) appears, indicating a typical pattern of an amorphous carbon structure in the r-GS, which is close to the d-spacing 3.36 Å of the graphite. The r-GS migrates to lower 2θ angles compared to the G, indicating the change of interlayer spacing [31]. This suggests that the interlayer spacing of r-GS layers (002) is larger in the r-GS than the G. Accordingly, these results suggest the chemical reduction happened successfully during the hydrothermal process [32].

Figure 4 presents the FTIR spectra of the G, GO, r-GO and r-GS samples. The spectrum of G shows a faint peak with the characteristic vibration of unsaturated C=C around 1570 cm^{-1}. Both GO and r-GO indicate a similar FTIR spectrum; broad bands at 3360 and 1624 cm^{-1} are respectively attributed to the stretching vibration of O–H groups (–COOH/–OH), while other peaks at 1716, 1580 and 1065 cm^{-1} correspond to the C=O, C=C and C–O stretching vibration, respectively. These demonstrate that the GO and r-GO possess abundant oxygen containing groups. After the reduction and self-assembly of r-GO by fructose, the intensities of all FTIR bands correlated to the oxygen containing groups decreased dramatically [33].

TEM was used to observe the structures on the nanoscale. Figure 5 presents the TEM images of the G, GO and r-GS samples. The G is tight aggregates within the host sheets, forming bulk nanostructural intergrowth, which exhibits lower interlayer spacing. As for the GO formation, the aggregated sheets dispersed to form thinner flaky, wrinkles and folds. The 3D network indicates the strong interconnection between building blocks. The r-GS exhibits a cellular structure inside with interconnected pores under microscopic observation. The pore walls are made up of assembled graphene sheets during the reduction and self-assembly process. This suggests that graphene sheets assembled to form larger sheets and then cross-linked to produce 3D porous structure. In addition, wrinkles and twists can be observed in the edges of the graphene sheets, which showed more wrinkles and folds than the GO. No carbon particle was found on the graphene sheets of r-GS. This was consistent with the literature results [34, 35].

SEM can be used to show the microscopic structures. Figure 6 presents the SEM images of the G, GO and r-GS samples. No obvious porous structure was observed for the G, while a rough morphological structure formed on the GO due to the packed thin layer sheets. As the GO sheets were reduced by fructose via hydrothermal treatment, the graphene sheets lost the dispersibility in an aqueous system, and the flexible graphene sheets overlap and coalesce with each other, forming a porous and well-defined 3D framework. The thinner cell walls or wrinkles inside the small pores may be responsible for the trapping and anchoring of organic molecules during the freeze drying, which is consistent with a previous report [36].

Figure 7 shows the Raman spectra of the G, GO, r-GO and r-GS samples. The spectrum of G shows a single line at 1578 cm^{-1} (G-band) and a faint D-band around 1340 cm^{-1} attributed to the graphite structure and amorphous structure, respectively. Moreover, the degree of structural order depends on the peak intensity ratio of I_D/I_G, where the value of the ratio decreases with the increasing degree of the carbon order. The D-band increased abruptly as the G was oxidized to form GO, and produced a large amount of defects. The Raman spectrum of GO, r-GO and r-GS exhibit similar characteristic intensities of G-band and D-band, while the intensity of G-band is weaker than that of D-band in the r-GS sample. The values of I_D/I_G for G, GO, r-GO and r-GS are 0.56, 1.00, 0.95 and 1.07, respectively.

The TPR technique is used to elucidate the reduction behavior of these carbon materials. Figure 8 shows the TPR profiles of the G, GO, r-GO and r-GS samples, and various degrees of reducibility are observed. Among these samples, the G is difficult to reduce, while the r-GO is easy to reduce. According to the literature [37, 38], the soft carbon can be reduced below 300 °C and the reduction temperature for the hard carbon exceeds 500 °C; the tendency of hardness is in the order of G > r-GS > GO > r-GO. From the reduction behavior, the oxygen-functional groups of –COOH/–OH belong to the soft species and the C–O–C functional group are attributed to the hard species.

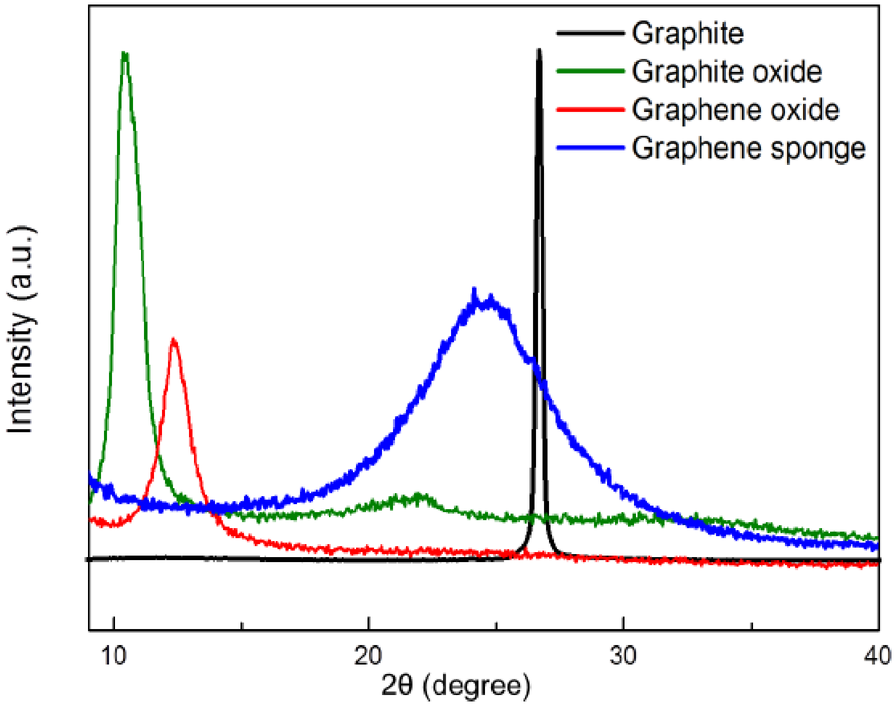

FIGURE 3. XRD patterns of G, GO, r-GO and r-GS samples.

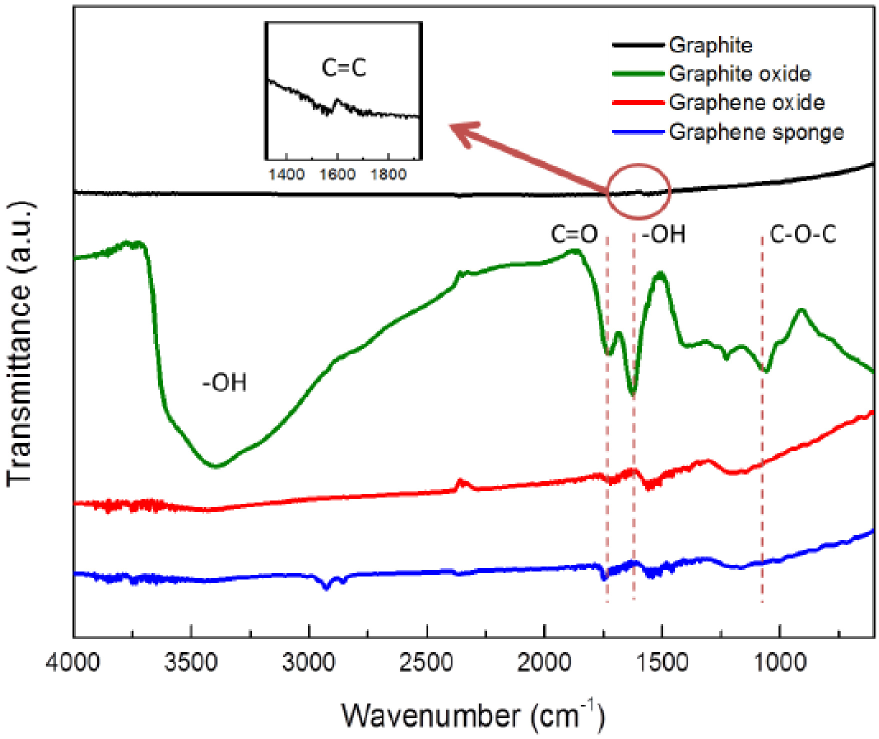

FIGURE 4. FTIR spectra of G, GO, r-GO and r-GS samples.

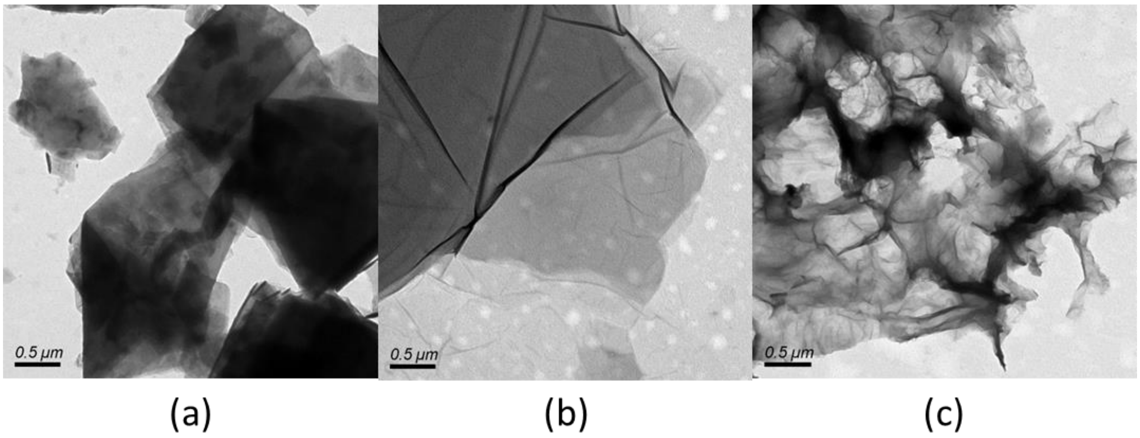

(a) (b) (c)

FIGURE 5. TEM images of (a)G, (b)GO and (c)r-GS samples.

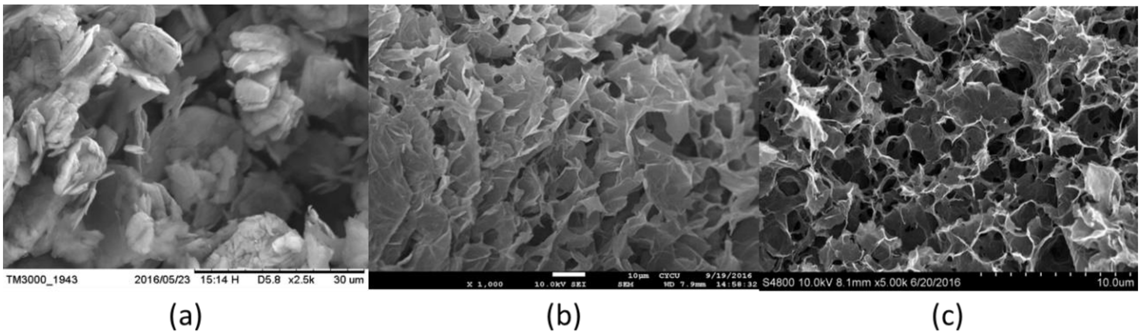

(a) (b) (c)

FIGURE 6. SEM images of (a)G, (b)GO and (c)r-GS samples.

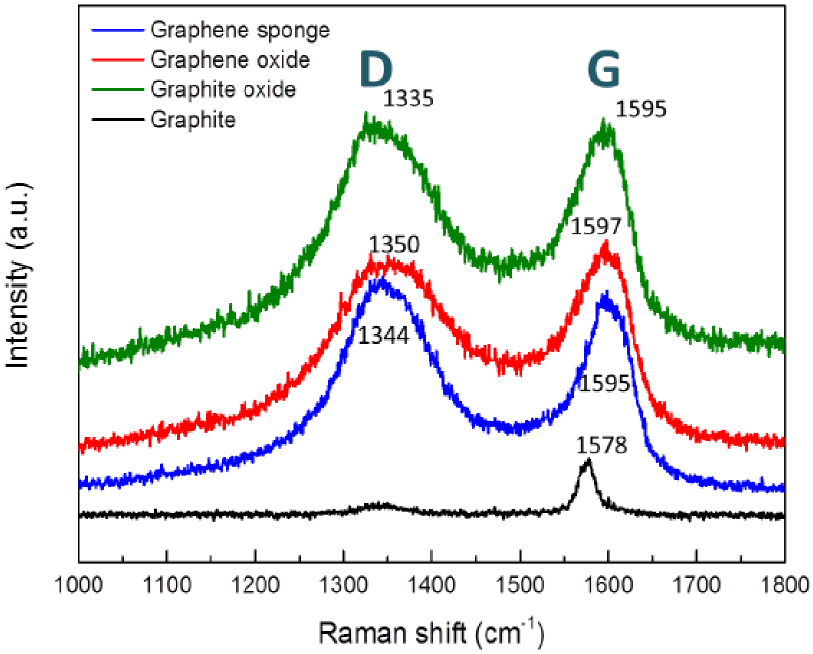

FIGURE 7. Raman spectra of G, GO, r-GO and r-GS samples.

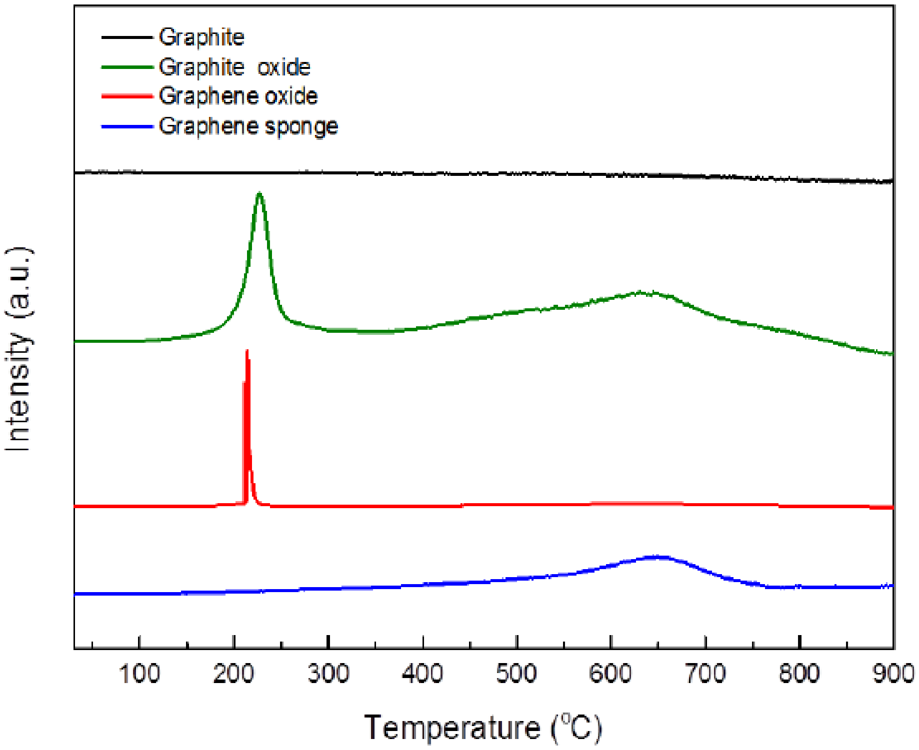

FIGURE 8. TPR profiles of G, GO, r-GO and r-GS samples.

Absorption capacity of oil and organic solvent by r-GS

Figure 9 displays the absorption capacities of r-GS on various oils and organic solvents, including vegetable and machine oils, ethanol, acetone and cyclohexane solvents. The absorption capacity was evaluated by weight gain, i.e. the ratio of total mass after absorption to the initial mass of r-GS. As shown in Fig. 9, the r-GS is capable of removing various pollutants. The absorption capacities are in the range of 15 ~ 38 g/g. The ultrahigh absorption performance indicates that the absorption is more like the accommodation of oils in the pores of the r-GS. In the absorption mechanism the pores should be hydrophobic, and the oils fill the micro- and macro- pores. In particular, the absorption capacity for vegetable oil is 37.8 g/g, indicating that the r-GS can be used for oil leakage treatment. Due to the remnant oxygen-functional group, the r-GS is also capable of the absorption of organic solvents, and polar solvents are preferable due to the very weak hydrophilicity of r-GS. For practical applications, the recycling of r-GS is very important for conventional treatment and reducing the operating cost. The regeneration of r-GS is achieved by burning. Figure 10 shows the regeneration of r-GS after the absorption of vegetable oil. Unfortunately, after 2 cycles, the absorption capacity dropped abruptly, about 22% of the raw r-GS in the preliminary results. At 10 cycles, the absorption capacity is only 12% of the raw GS. This phenomenon may be attributed to the worse mechanical properties of cross-linked graphene nanosheets in influencing the microstructures on the regeneration by burning. In the future, we will try to tune the parameters of synthesizing r-GS, such as by the kinds of reducing agents and the ratio of concentration, temperature and time of hydrothermal process, and the temperature in the freeze drying process. Also, the regeneration by various methods will be pursued.

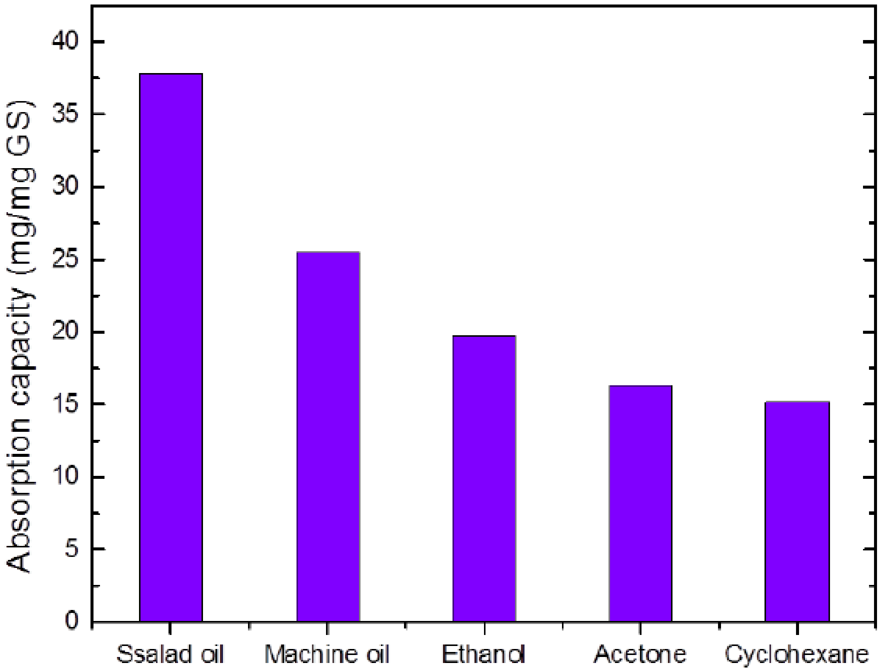

FIGURE 9. Absorption capacities of r-GS towards various oils and organic solvents.

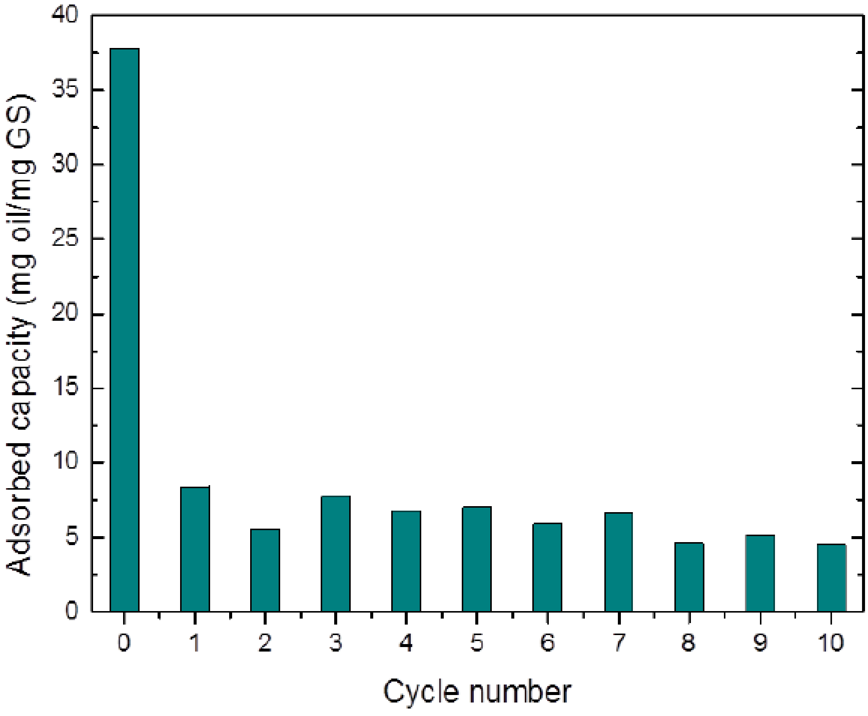

FIGURE 10. Regeneration of r-GS after the absorption of vegetable oil.

Conclusions

With the combination of fructose surfactant and freeze-drying, we have developed a facile preparation of r-GS with a highly enhanced performance as oil sorbent. The absorption capacities are in the range of 15 ~ 38 g/g for various oils and organic solvents, while the capacity of regeneration is worse in the preliminary stage. So, the regeneration by various methods will be pursued. We hope that our study will stimulate more interest in graphene-based environmental nanotechnologies, and open up many possibilities for the use of graphene in water cleaning, including decontamination, reuse and reclamation.

Acknowledgements

We are pleased to acknowledge the financial support for this study from the Ministry of Science and Technology of the Republic of China under contract number of MOST 105-2119-M-606-001-.

References

1. C. Ramesh, J. Banerjee, R. Pal and B. Das, Adv. Synth. Catalysis **345**, 557-559 (2003).
2. S. R. Sheng, Q. Y. Wang, Y. Ding, X. L. Liu and M. Z. Cai, Catal. Letters **128**, 418-422 (2009).
3. K. Reddi Mohan Naidu, B. Satheesh Krishna, M. Anil Kumar, P. Arulselvan, S. Ibrahim Khalivulla and O. Lasekan, Molecules **17**, 7543-7555 (2012).
4. J. Xu, H. Lv, S. T. Yang and J. Luo, Rev. Inorg. Chem. **33**, 139-160 (2013).
5. K. C. Kemp, H. Seema, M. Salah, N. H. Le, K. Mahesh, V. Chandra and K. S. Kim, Nanoscale **5**, 3149-3171 (2013).
6. Y. Cao and X. Li, Adsorption **20**, 713-727 (2014).
7. L. Zhao, B. Yu, F. Xue, J. Xie, X. Zhang, R. Wu, R. Wang, Z. Hu, S. T. Yang and J. Luo, J. Hazard. Materials **286**, 449-456 (2015).
8. B. Yu, X. Zhang, J. Xie, R. Wu, X. Liu, H. Li, F. Chen, H. Yang, Z. Ming and S. T. Yang, Appl. Surf. Science **351**, 765-771 (2015).
9. M. Fang, K. Wang, H. Lu, Y. Yang and S. Nutt, J. Mater. Chem. **19**, 7098-7105 (2009).
10. D. R. Dreyer and C. W. Bielawski, Chem. Science **2**, 1233-1240 (2011).
11. Y. F. Li, M. Q. Guo, S. F. Yin, L. Chen, Y. B. Zhou, R. H. Qiu and C. T. Au, Carbon **55**, 269-275 (2013).
12. D. H. Lan, F. M. Yang, S. L. Luo, C. T. Au and S. F. Yin, Carbon **73**, 351-360 (2014).
13. D. H. Lan, L. Chen, C. T. Au and S. F. Yin, Carbon **93**, 22-31 (2015).
14. M. J. Allen, V. C. Tung and R. B. Kaner, Chem. Rev. **110**, 132-145 (2010).
15. W. S. Hummers and R. E. Offeman, J. Am. Chem. Soc. **80**, 1339-1339 (1958).
16. Y. Liu, X. Dong and P. Chen, Chem. Soc. Rev. **41**, 2283-2307 (2012).
17. B. F. Machado and P. Serp, Catal. Sci. Technol. **2**, 54-75 (2012).
18. H. Bi, X. Xie, K. Yin, Y. Zhou, S. Wan, L. He, F. Xu, F. Banhart, L. Sun and R. S. Ruoff, Adv. Funct. Materials **22**, 4421-4425 (2012).
19. J. Zhao, W. Ren and H. Cheng, J. Mater. Chem. **22**, 20197-20202 (2012).
20. H. Bi, X. Xie, K. Yin, Y. Zhou, S. Wan, S. R. Rodney and L. Sun, J. Mater. Chem. A **2**, 1652-1656 (2014).
21. S. Pourmand, M. Abdouss and A. Rashidi, J. Ind. Eng. Chem. **22**, 8-18 (2015).
22. T. Ricky, L. Gregory, V. Alicia, B. Josh, C. Gordon and Y. Aiping, Ind. Eng. Chem. Res. **54**, 3657-3663 (2015).
23. X. Yang, C. Chen, J. Li, G. Zhao, X. Ren and X. Wang, RSC Adv. **2**, 8821-8826 (2012).
24. J. Zhao, Z. Y. Wang, J. C. White and B. S. Xing, Environ. Sci. Technol. **48**, 9995-10009 (2014).
25. T. Maiyalagan, X. Dong, P. Chen and X. Wang, J. Mater. Chem. **22**, 5286-5290 (2012).
26. Y. Liu, J. Ma, T. Wu, X. Wang, G. Huang, Y. Liu, H. Qiu, Y. Li, W. Wang and J. Gao, ACS Appl. Mater. Interfaces **5**, 10018-10026 (2013).
27. B. Ge, Z. Zhang, X. Zhu, X. Men, X. Zhou and Q. Xue, Compos. Sci. Technol. **102**, 100-105 (2014).
28. S. Zhou, W. Jiang, T. Wang and Y. Lu, Ind. Eng. Chem. Res. **54**, 5460-5467 (2015).
29. S. Yang, L. Chen, L. Mu and P. C. Ma, J. Colloid Interface Science **430**, 337-344 (2014).
30. G. Wei, Y.E. Miao, C. Zhang, Z. Yang, Z. Liu, W. T. Weng and T. Liu, ACS Appl. Mater. Interfaces **5**, 7584-7591 (2013).
31. W. F. Chen and L. F. Yan, Nanoscale **3**, 3132-3137 (2011).
32. R. Li, C. Chen and J. Li, J. Mater. Chem. A **2**, 3057-3064 (2014).
33. G. Wang, B. Wang and J. Park, Carbon **47**, 68-72 (2009).
34. C. C. Ji, M. W. Xu, S. J. Bao, C. J. Cai, Z. J. Lu, H. Chai, F. Yang and H. Wei, J. Colloid Interface Science **407**, 416-424 (2013).
35. W. Tang, L. Peng, C. Yuan, J. Wang, S. Mo, C. Zhao, Y. Yu, Y. Min and J. E. Arthur, Synth. Met. **202**, 140-146 (2015).
36. X. Xie, Y. L. Zhou, H. C. Bi, K. B. Yin, S. Wan and L. T. Sun, Sci. Rep. **3**, 2117 (2013).
37. V. A. Tsipouriari and X. E. Verykios, J. Catalysis **179**, 292-299 (1998).
38. K. H. Lin, C. B. Wang and S. H. Chien, Int. J. Hydrogen Energy **38**, 3226-3232 (2013).